平成20年度博士論文

三波川変成岩のシールドクラック様式とプレート境界の流体・変形結合

Mode of sealed-cracks in the Sanbagawa metamorphic rocks and fluid-deformation coupling in the plate boundary

氏名　　玉原正之

専攻　　複雑理工学

学生番号　47-57407

指導教官　鳥海光弘 教授

Contents

1 Introduction

1.1 Asperity and heterogeneity

In the subducting plate boundary regions, the oceanic plates are subducting from the trench beneath the continental or other oceanic plates and toward the Earth's interior. As a case of the situation near Japan, North American and Philippine sea plates are the oceanic plates, Eurasian plate is continental plate, and Japan trench, Izu-Ogasawara trench, and Nankai trough are the trenches. The subducting plates had been thought to stick fast uniformly to the continental plates, where the former drags the latter down together. However, the detailed stick state between the plates has been clarified by the recent progress in seismological observation mainly encouraged by the dense seismometer network and the verified analyses on waveform of earthquakes. According to it, there are some spatial variations in the stick state between the plates. One region which sticks strongly in usual, and slips rapidly and releases strong short period seismic wave in an earthquake is called "asperity", and the other "slow slip region" (Fig.1-1).

In recent years earthquake occurrence phenomenon in the plate bound-

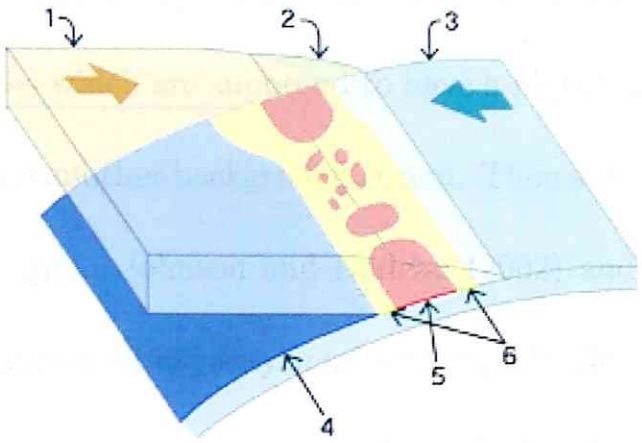

Figure.1-1 Proposed cross section view and heterogeneity structure near a subduction trench. Symbols: 1.continental plate 2.accretionary wedge 3.oceanic plate 4.stable slip region 5.stick region (asperity) 6.slow slip region.

aries have been understood commonly by the asperity model which is one of the greatest progress on earthquake predicting research in last decades (Lay and Kanamori 1980, 1981; Aki 1984; Cloos 1992; Sammis *et al.* 1999; Lei *et al.* 2000; Johnson and Nadeau 2002; Chen and Sammis 2003; Yamanaka and Kikuchi 2003; Wells *et al.* 2003; Seno 2003; Kawasaki 2004; Okada *et al.* 2005; Sobiesiak *et al.* 2007). The classical asperity model as introduced by Lay and Kanamori (1980,1981) describes heterogeneous stress distributions on fault planes of large subduction zone earthquakes, assuming a varying degree of seismic coupling between the downgoing and overriding plate, which has been examined quantitatively using the earthquake catalogue covering all type plate boundaries by Brune (1968)

and Bird and Kagan(2004). The two plates are more strongly coupled through asperities which are supposed to have a higher friction coefficient and strength than another background region. Then some asperity models have been developed. Johnson and Nadeau (2002) and Chen and Sammis (2003) presented an asperity model to explain the empirical scaling relationships for repeating earthquakes along the San Andreas fault in central California, assuming that the asperity patches are distributed on the fault surface in a random fractal manner which leads to a frequency-size distribution of earthquakes (the Gutenberg-Richter formula) and a simple relationship between the b-value and the fractal dimension proposed by Sammis (1999). Seno (2003) presented an asperity model to explain variation of seimicity along same subducting plate boundaries based on the assumption of fractal asperity manner and fluid invasion of barrier structures proposed by Aki (1979, 1984). Kawasaki (2004) indicated that the slow-slip-events are separated from the major asperities, where silent earthquakes are different from ordinary earthquakes in source parameters, source time functions, and moment release rate. Therefore there seems to be difference in the circumstance between asperities and back ground regions in a plate boundary. It is important to understand what may

make them different, which can explain together the difference such as the frictional a-b parameters.

So far not very much has been known clearly about the nature of asperity. Resulting heterogeneity of the coupling has been considered inherent in each plate boundary with geological structure. As similar earthquakes occur repeatedly in nearly same location and time interval, Yamanaka and Kikuchi (2003) and Okada (2005) suggested the heterogeneity may be undisturbed during at least some earthquake cycles. Therefore the difference in a manner of the earethquakes (magnitude, location, aftershock sequence) is interpreted to come automatically from a combination of ruptured asperities.

However, the variability of time interval of main large shock and its moment release evokes the space-temporal variation of circumstance near large asperity or coupling situation of small asperities in relatively short time period. The variation model of small asperities and resulting moment release can be meaningful than stochastic rupture one of immobile asperities. As for the immobility of main large asperity, the fixed local large strength structure such as a subducting seamount gives one of the convincing answer (Cloos 1992; Wells *et al.* 2003). Sobiesiak *et al.*

(2007) suggested actual main large asperity in Chile Trench is strongly locked stably between gabbroic batholithic structures heavier than the surrounding crust and mantle buoyant force, inferred from the observation of gravitational anomaly. Lei *et al.* (2000) also suggested in natural rock experiments the large quartz vein works as main asperity, showing other earthquake-like phenomenon such as precursor, concentrating acoustic emission, dilatancy, b-value variation.

1.2 Asperity and b-value variation

The number of earthquake N of magnitude equall or greater than M per appropriate time interval is observed to follow a simple relationship named the Gutenberg-Richter relation (Gutenberg and Richter 1944, Ishimoto and Iida 1939)

$$\log_{10} N = a - bM \tag{1.1}$$

where a is the corresponding level of seismic activity and b is the slope which takes the value $b \approx 1$ usually in a large space and time window but varies locally depending on the situation investigated. Numerical values of the coefficients, $a = 8.0 \pm 0.2$ and $b = 1.00 \pm 0.03$, from a global data for $4 < M < 8$ were fit by Kanamori and Brodsky (2004). There

must be limits to the magnitude range to which this applies. Although suggestions of a lower limit have appeared in the literature, studies with modern instruments, especially in deep boreholes, showed that Eqs.(1.1) is valid down to at least $M = 0$ (Abercrombie 1995, 1996). It is not clear that there is any lower limit short of the scale of grain boundaries in rocks.

Local variations in spatial seismic b-value distribution can represent changes in the state of stress and in material property. This dual capability of b-value could evidenced in laboratory experiments, induced seismicity and seismotectonic studies. In micro- and macro scale environments b-value seems to react on crack or rupture densities, which results from the amount of applied stress or pressure, type of material and rupture dynamics. Hence b-value is usually used to map out inhomogeneities in seismogenic fault areas which can be attributed to potential asperities (Wiemer and Wyss 1997; Hirose *et al.* 2002; Westerhaus *et al.* 2002; Amitrano 2003; Wyss *et al.* 2004; Schorlemmer *et al.* 2005). Wiemer and Wyss (1997) for instance described that areas of low-b values with a size range of 5-15km correlate with asperities in the Parkfield and Morgan Hill sections of the San Andreas Fault. This hypothesis that low-b values indicate asperities on the falut prior to a large earthquake is supported by

the study of Wyss *et al.* (2004) showing that *b*-values on locked patches of the San Andreas Fault near Parkfield are systematically lower than them on creeping patches. Hirose *et al.* (2002) and Westerhaus *et al.* (2002) suggested a clear temporal *b*-value variation associated with the rupture of asperities which are separated clearly from steady high *b*-value regions and indicate low *b*-values before large main shocks and a remarkable high *b*-values after the rupture of each asperity. This observation is a direct consequence of the inverse relationship of *b*-value to the applied shear stress, suggested by Amitrano (2003) and Schorlemmer *et al.* (2005) who are saying that the high-sterss environment of locked fault patches is more likely to support future large earthquake occurence.

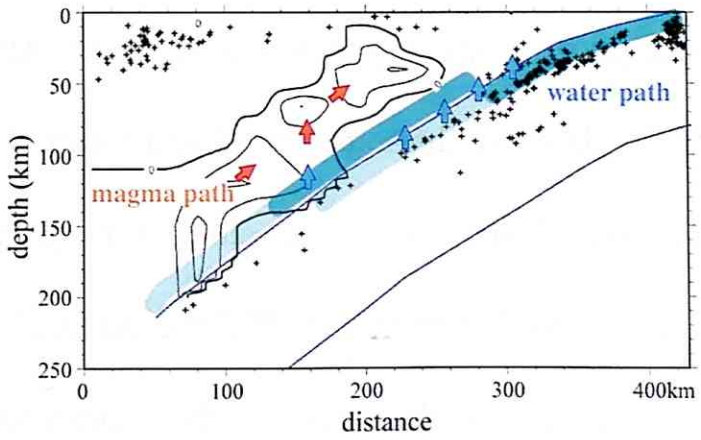

Figure.1-2 Fluid circulation image in the subduction zone beneath Tohoku northwest Japan with seismic tomography techniques from Kawakatsu and Watada (2007). Contour shows low seismic wave velocity areas.

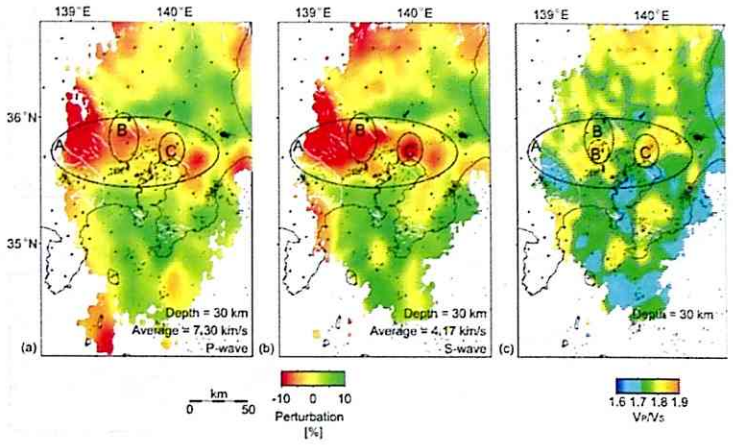

Figure.1-3 Horizontal cross sections beneath the Kanto area at a depth of 30km from Matsubara *et al.* (2005) (a)Vp perturbation (b) Vs perturbation (c)Vp/Vs ratio.

1.3 Crack filled with fluid

Fluid circulation in subduction zones plays an important role on the mechanical response of the crust to earthquakes. Recently physical images of water and other fluid are given to a depth of upper mantle, where dehydration occurs mainly on peridotite, by seismic tomography techniques. According to it water can be transported to the depth and circulate to the surface through the whole subduction zone (Fig.1-2) (Kawakatsu and Watada 2007; Iwamori 2007; Hasegawa and Nakajima 2004).

Seismic tomography techniques have elucidated the velocity and Vp/Vs structures in the plate boundary. It shows the distinguished low velocity and high-Vp/Vs patches (Fig.1-3). Although if the structure of anomalous patches are beneath volcanoes it can be derived from magma and following

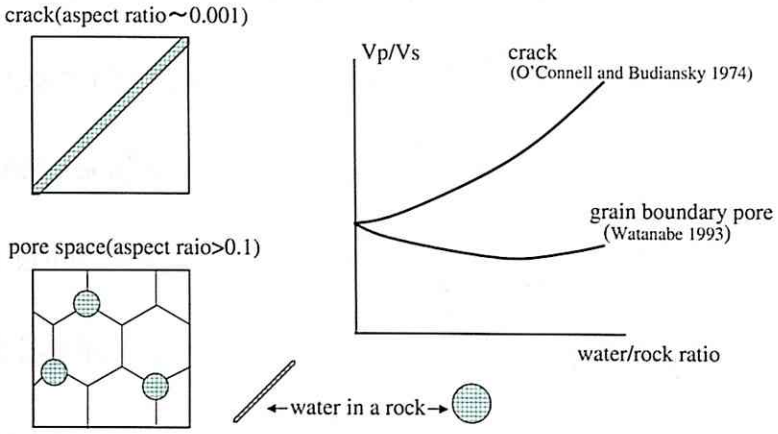

Figure.1-4 Efficiency to Vp/Vs of the shape (aspect ratio) of water in a rock.

water, in not the case it will be possible only from dehydrating water from the subducting slab. Here need be considered that the effect of water to the Vp/Vs ratio depends on shapes of water in a rock. How rocks contain fluid can roughly be classified into two end members. One is storing it within pore spaces of grain boundaries of a rock, the other within cracks newly made or pre-existing there. Two water shapes in a rock are different in aspect ratio and the efficiency to Vp/Vs value. Vp/Vs ratio of the rock containing the cracks filled with water increases rapidly even in a little water/rock ratio, whereas in the pore spaces it doesn't vary significantly (Fig.1-4) (O'Connel and Budianski 1974; Watanabe 1993; Takei 2002). Consequently the high-Vp/Vs anomaly is easily understood as high water content and highly cracked zone.

The temporal-spatial Vp/Vs variation with water is utilized as a means

to observe variety of water-related earthquake phenomena as well as b-value. For example Husen and Kissling (2001) investigated Vp/Vs ratio obtained from local earthquake tomography on a earthquake cycle in the subduction zone, Antofagasta, Chile, and observed high-Vp/Vs after the main shock in the region of the proposed large asperities, suggesting that this is caused by fluid intruding into the fractured material. This process might cause additional fracturing expressed by the occurrence of further small aftershocks and high b-value (Shapiro *et al.* 2003).

Cracks filled with water give heterogeneity to not only wave velocities but strength, permeability, and so on. Therefore a series of hypotheses above about the relation between rupture or fracture and water need be tested in natural rocks recording the situation, namely metamorphic rocks containing the sealed cracks in subducting plate boundaries, which were clearly the fluid-filled cracks. This paper provides the information about the mode of the sealed cracks in the Kanto Mountains, the Sanbagawa metamorphic belt, Japan and some models to understand it, which can constrain the spatio-temporal variation of heterogeneity in the plate boundary.

1.4 Sealed-crack

Sealed-cracks are called veins normally. Veins occur in many forms, are composed of many different minerals and occur at all levels of the Earth's crust and mantle. Their morphology, petrology and chemistry is a valuable source of information in a range of geological disciplines. The association of many ore deposits (particularly gold) with veins makes them even more relevant to geology. It is therefore not surprising that veins have been studied extensively. Yet, the formation of veins is still not fully understood. One surprising aspect of veins is that no one has been able to successfully and consistently simulate the formation of the variety of vein types - not in real rocks, nor in rock analogues. Attempts with varying degrees of success have certainly been made by those such as Hilgers and Urai (2005), Nollet *et al.* (2005), Hilgers *et al.* (2003) and so forth.

Because of compressional stress in the deep ground, it is necessary for pore pressure P_{f} to push back from the inside of the rock for making new mode I cracks. Universal currency of the cracks sealed with minerals in the metamorphic rocks suggests the important role of hydrothermal aqueous fluid or water. For making new cracks without leakage into the rock fluid are needed to be a high content level to near the critical value and high

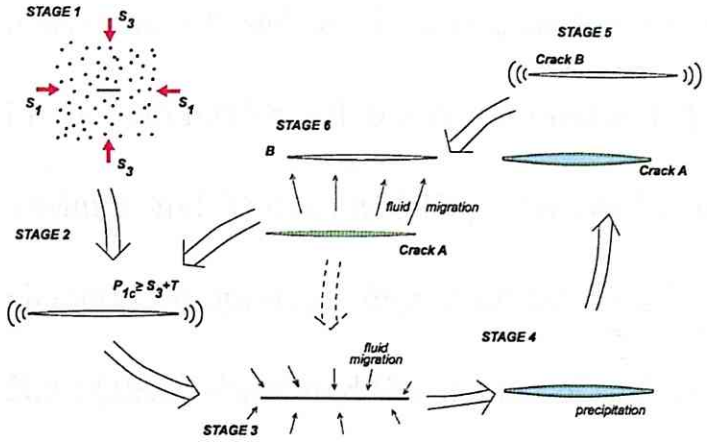

Figure.1-5 Commonly-used sealed crack formation scenario by the serial processes of crack growth, pressure drop and fluid migration from Etheridge *et al.* (1984)

flow velocity (Nakashima 1995). It is supposed normally to be achieved by a large amount of upgoing fluid through the rock supplied from the subducting slab (oceanic plate and sediments) by dehydration reactions (metamorphic dewatering) in high-P,T condition (Okamoto and Toriumi 2005; Toriumi and Inui 2001; Winstch *et al.* 1999). The commonly-used sealed crack formation scenario is by the serial processes of crack growth, pressure drop and fluid migration under the assumption of nearly saturated pore pressure in the host rock (Etheridge *et al.* 1984) (Fig.1-5). Also in this paper, this scenario is adopted basically and fluid is assumed to be fully supplied as the occasion demands.

Fluid in the crust usually flows in rocks. As a path, porous (pervasive) flow and crack (channelized) flow are considered. Crack flows have been

investigated based on the fact that there are many sealed-cracks (veins) in the subduction related metamorphic belts (Toriumi and Hara 1995; Toriumi and Yamaguhi 2000). Group feature of the cracks, especially clustering property, is important for fluid flow in the crust. Toriumi and Hara (1995) elucidated the manner of sealed-cracks within the Sanbagawa metamorphic rock in the Kanto-Mountains with metamorphic grade from chrolite to biotite zone and reported that thickness (width), length, and spacing frequency distributions take power-law forms. Thus cracks in the crust are expected to make highly clustered structure. Toriumi and Yamaguchi (2000) described the temporal and space developing model of the crack systems, in which the master equation of number density of the cracks have a non-linear term and scale- and time-invariant solutions of two-thirds power exponents. The clustering property predicted by the model is comparable to the result 0.7-0.9 fractal dimensions in 1-D for spacing by Toriumi and Hara (1995). In the clustering crack systems, the power exponents D among thickness, length and spacing are expected to have correlation relations similar to those of earthquakes among fractal dimension Dc, p-value of modified Omori formula and b-value of Gutenberg-Richter relation (Guo and Ogata 1997; Vinciguerra 2002). Whether the

correlation patterns in the crack systems are constructed in natural system is also important for the scale problem of fracture phenomena.

Geometry of sealed cracks are also thought a recorder of the fracture processes. Toriumi and Hara (1995) analyzed the geometry of the sealed cracks in the metamorphic rocks and reported that the geometrical factor m-value of $W = kL^m$, where W is width (thickness), L length and k constant, of the sealed cracks get larger (fattened) with the metamorphic grade. Nüchter and Stöckhert (2007) and Birtel and Stöckhert (2008) suggested that the shape of discordant quartz veins with large thickness formed at temperatures of about 500 to 550°C could not indicate intensive hydrofracture but inhomogeneous ductile deformation of the host rock during opening and sealing controlled by the presence of the cohesionless fluid-filled fractures.

The sealed crack microfabrics are also related to the processes. Toriumi and Hara (1995) reported that the average quartz grain size have a linear relation with a thickness smaller than 1mm of the sealed crack, and suggested the balance between the incremental opening rate of the crack and mineral sealing rate. Birtel and Stöckhert (2008) showed that the discordant vein quartz microfabrics indicate crystallization in an open cavity,

implying a stage of very high permeability and fluid flow. They argued that the event of brittle failure at 500 to 550°C followed by an episode of inhomogeneous ductile deformation is attributed to stress changes related to the earthquake cycle, i.e. coseismic loading and postseimic creep. Consequently geometry and microfabric are important and need to be investigated here as one of the mode of the sealed cracks.

2 Geological Setting

Geology of the whole Sanbagawa metamorphic belt and the Kanto Mountains, which is a part of the belt, is outlined here. In the comparison with the Kanto mountainous, Shikoku district as more advanced region for the geological research is outlined, too.

2.1 Distribution

The Sambagawa (Sanbagawa) metamorphic belt is one of the most representative subduction-related high-pressure metamorphic belts in the world, which extends about 800km from easten Kyusyu to Kanto Mountains (Fig.2-1). The northern limit of the Sambagawa belt is clearly defined by a major strike-slip fault, the Median Tectonic Line (M.T.L.), and is bordered by Ryoke high-temperature metamorphic belt. M.T.L. directly divides the Ryoke and Sambagawa metamorphic belts, but in central and eastern Shikoku the region immediately to the north of the M.T.L. is occupied by the Izumi Group which is composed of dominantly coarse-grained classics which overlies the Ryoke metamorphic belt. To the south, the Sambagawa belt is bounded by the Northern Chichibu belt. The boundary between the Sambagawa and the Northern Chichibu

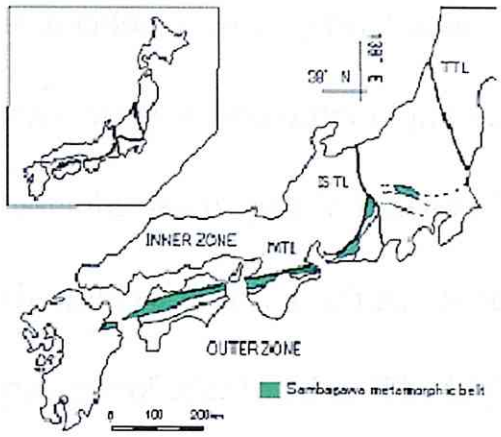

Figure.2-1 Sambagawa metamorphic belt

belt is usually located along the southern limit of a prominent greenstone belt, the Mikabu Greenstone belt.

The width of the belt in central Shikoku is around 30km, and in the Kanto Mountains is 60km from Ogose-mati, Saitama to Shimonita-mati, Gunma. There are abundant good exposures of the metamorphic sequences from the lowest grade to the highest grade. The rocks are dominantly composed of pelitic and basic schists accompanied with small amounts of psammitic and siliceous schists, and rare calcareous schists. Higher grade-mafic and -ultramafic masses are locally found.

2.2 Metamorphic zonal structure

Metamorphic zonal structures of the Sambagawa metamorphic belt in Shikoku where researches have been achieved energetically are divided

into chlorite zone, garnet zone, albeit-biotite zone, and oligoclase-biotite zone in ascending order of present remained temperature based on mineral assemblages of pelitic schists (Higashino 1975, 1990; Enami 1982). The thermal structure is almost accordance with the geological structure and posture of schistosities. The highest grade zone is distributed in the structural middle position, from which metamorphic grade declines to upper and lower direction.

In the Kanto Mountains of the Sambagawa metamorphic belt, metamoprhic zonal structures of pelitic schists are divided into chlorite zone, garnet zone and biotite zone based on mineral assemblages and its degree of graphitization (Fig.2-2) (Tanaka and Fukuda 1974; Sakai 1980; Tokuda 1986; Hashimoto and Funakoshi 1991; Hashimoto *et al.* 1992; Yano and Tagiri 1998; Miyashita 1998; Abe *et al.* 2001; Tagiri *et al.* 2003). And also the metamorphic facies are reported to extend from pumpellyite-actinolite facies to epidote-amphibolite facies (Toriumi 1975; Hirajima *et al.* 1992). The highest grade zone of the Sambagawa metamorphic belt in the Kanto Mountains is also distributed in the structural middle position as same as Shikoku. The thermal structure, however, is disturbed partly and not accordance with the geological structure. Hashimoto *et al.* (1992) showed

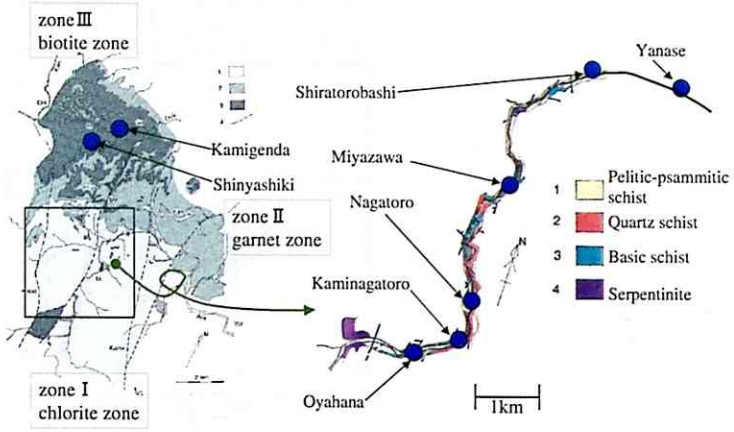

Figure.2-2 Metamorphic zonal structures in the Kanto-Mountains of the Sambagawa metamorphic belt (left) and rock type facies along the Arakawa-river with the sites investigated here (right) from Hashimoto *et al.* (1992).

that zone Ⅱ (garnet zone) and zone Ⅲ (biotite zone) bodies determined by the degree of graphitization appear lenticularly in zone I area. It was interpreted that the primary thermal and geologic structure of metamorphism is not preserved and the metamorphic terrain has been formed by tectonic stacking of a number of thin layers having characteristics of each zone sliced after metamorphism as so called shuffled-cards structure (Miyashiro 1994). Miyashita (1998) reexamined the strange structure by mineral isograde and Mg-Fe partition coefficient and did not agree with the model of Hashimoto *et al.* (1992). This problem has been discussed to date (Yano and Tagiri 1998; Tagiri *et al.* 2003).

P-T paths of the Sambagawa metamorphic rocks have long been discussed by many workers (Banno *et al.* 1986; Otsuki and Banno 1990;

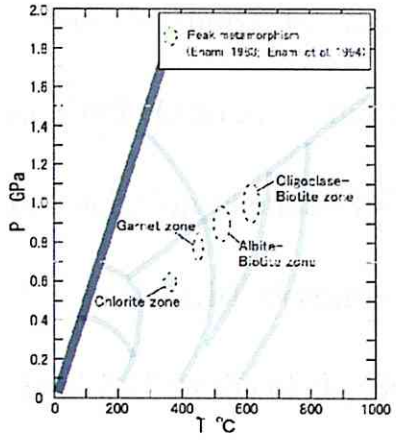

Figure.2-3 Metamorphic P-T conditions corresponding to the metamorphic grades of the Sanbagawa belt estimated from the mineral assamblage.

Nakamura and Enami 1994; Enami 1998; Banno 2000; Tagiri *et al.* 2000; Okamoto and Toriumi 2001, 2004; Inui and Toriumi 2002). Peak pressure and temperature conditions are estimated from matrix mineral composition by using different geothermobarometers for different metamorphic grade rocks in Shikoku(Enami 1983; Enami *et al.* 1994), although results are including errors derived from modification of matrix mineral compositions during retrograde metamorphism and difference of geothermobarometer (Fig.2-3). Depending on those, pressure has extended about 8-10kbar and temperature about 400 ℃, 450 ℃, 550 ℃, and 600 ℃ for chlorite zone, garnet zone, albeit-biotite zone, and oligoclase-biotite zone, respectively. The conditions of the Kanto Mountains are assumed to be almost same as Shikoku, corresponding to the metamorphic zonal structures of the Sambagawa regional metamorphism. Recently rigorous quantitative P-T

paths are shown for the Sambagawa metamorphic belt by using Gibbs' method (Okamoto and Toriumi 2001, 2004; Inui and Toriumi 2002) and by inclusion chemistry (Aoya *et al.* 2003). In contrast to the previous P-T paths with decompression heating (e.g., Enami 1998), the newly derived P-T paths of the Sambagawa metamorphic belt suggest that garnet zonings record subduction processes (Inui and Toriumi 2002; Aoya *et al.* 2003) and exhumation processes can be estimated by amphibole zoning (Okamoto and Toriumi 2001, 2004). According to thermal modeling of subduction zone, it becomes clear that P-T paths of the Sambagawa metamorphic rocks are similar to the metamorphic conditions of younger subducting plate than 1-5 Ma(Peacock and Wang 1999; Iwamori 2000; Aoya *et al.* 2003). Above studies for P-T paths of the Sambagawa metamorphic rocks, the study for thermal condition of subduction zone and slab age during the metamorphism has been developed remarkably.

2.3 Geochronology

Many microfossils (radiolarians and conodonts) have been described from the Sambagawa belt and the Mikabu Greenstone belt in western Shikoku. These fossils suggest ages of Carboniferous (Suyari *et al.* 1980a), middle

to late Triassic (Suyari *et al.* 1980b), and late Jurassic (Iwasaki *et al.* 1984). In the Kanto Mountains, radiolarians and pentacrinites have been seen in red shales and calcareous schists (Fujimoto 1939; Fujimoto and Yamada 1949; Guidi *et al.* 1984). However, those as such cannot determine a correct geological age. Isotopic ages have been also reported for samples from the Sambagawa belt, many of which have been collected in western Shikoku. Itaya and Takasugi (1988) reported 60-80Ma K-Ar age for muscovite and show gradual younging with decreasing metamorphic grade. Takasu and Dallmeyer (1990) reported 40Ar/39Ar ages of amphiboles, muscovite and whole-rock samples. The age recorded in amphibole of the albite-biotite zone (84-87Ma) is similar to those recorded in muscovite of this zone. On the other hand, the age of 94Ma recorded in amphibole of the oligoclase-biotite zone is significantly older than muscovite ages of the same zone. Thus, it seems that the rocks of oligoclase-biotite zone have passed through the closure temperature of amphiboles (approximately 500 ℃) earlier than the albite-biotite zone rocks. On many radiometric study, the fossil data should suggest that the protoliths of the Sambagawa belt had accumulated in accretionary wedge at the latest Jurassic, probably around 120-130Ma (Isozaki and Itaya 1990). As a peak metamorphic age,

116Ma Rb-Sr whole rock isochron age has been reported for pelitic schists of the albite-biotite zone. After that, the retrograde metamorphism associated with a formation of sealed cracks is supposed to occur from 110Ma to 60Ma.

2.4 Structure

The Sambagawa metamorphic belt has undergone high-strain ductile deformation characterized by a stretching direction that is roughly parallel to the trend of the belt (Toriumi 1982, Faure 1983, Faure 1985, Shimizu and Yoshida 2004). This is the dominant phase of ductile deformation in the Sambagawa metamorphic belt and is labeled D_1, D_S or the pre-Nagahama phase (fold) by most workers (e.g. Hara *et al.* 1977). At least two discrete phases of folding, D_2 and D_3 that occurred after D_1 can be identified. Although both D_2 and D_3 folds have axes that run approximately parallel to D_1 linear structure, these phases clearly deform the D_1 schistosity. D_2 axial planes are generally inclined gently to the north whereas D_3 axial planes are generally subvertical.

Pre-D_1 deformation is poorly preserved and any kinematic indicators will have suffered an unknown amount of rotation. D_1 structures are very

clearly developed. The most characteristic feature is the roughly E-W stretching lineation. Kinematical analyses of D_1 deformation have been carried out in several parts of the Sambagawa metamorphic belt (Toriumi and Noda, 1986; Shimizu 1988; Hara *et al.* 1990). In central Shikoku the sense of shear during D_1 was determined using quartz c-axis fabrics, shear bands, asymmetric pressure shadows, and locally the distribution of deformed veins (Wallis *et al.* 1992). Toriumi (1985) and Toriumi and Noda (1986) suggested that the regional total ductile strain of the Sambagawa belt is characterized by constructional finite strain approximating to uniaxial extension, based on quantitative strain analysis. The data presented by Toriumi (1985) are taken from deformed radiolarians in the low-grade regions of the Sambagawa metamorphic belt. Its results are extrapolated to discuss the state of finite strain in the whole Sambagawa metamorphic belt.

In central Shikoku, the highest-grade rocks are exposed in structurally middle layer and the lower grade rocks surround the highest grade layer. This type of thermal structure of the Sambagawa metamorphic belt in central Shikoku has been interpreted by the piles of nappe accompanying thrust faults (Hara *et al.* 1977; Faure 1983, 1985; Hara *et al.* 1990,

1992; Higashino 1990; Takasu *et al.* 1994) or large south vergent recumbent fold (Banno *et al.* 1978; Banno and Sakai 1989; Wallis 1990; Wallis *et al.* 1992). It was considered that the present thermal structure has formed in the process of the exhumation of the Sambagawa belt. As mentioned above, however, the notable discontinuities of Fe-Mg partitioning between garnet and chlorite have not been detected at the metamorphic zone boundaries (Higashino 1990). The lack of large breaks in the metamorphic sequence suggests that faulting has not had a major effect on the structure of the high-grade region (garnet zone and higher grade material).

In the Kanto Mountains, the highest-grade layer is also laid in the middle position as Shikoku. Foliation of the rock inclines a little or is nearly parallel. Some workers have thought the thermal structure to be harmonic with the geological structure (Tokuda 1986).

3 Description of the sealed crack

Sealed cracks are clearly derived from fluid-filled cracks. Some crack formation machanisms on which fluid plays an important role have been proposed due to a variety of circumstances. Fluid transports material into the cracks following mineral sealing. As sealing minerals are precipitated from aqueous fluid, it is clear that materials are transported in solution and that supersaturation for the minerals are achieved in the fluid filled crack. How and why material can be transported in solution to cracks, and why at some stage the fluid may be supersaturated and precipitate sealing minerals are outlined below briefly in keeping with Oliver (2001). Next the sealed cracks investigated here are described.

3.1 Sealed crack formation mechanisms

Transport and precipitation are not always independent processes but a division is attempted here for clarity. Transport mechanisms are classified into three groups, that is, diffusional flow through fluid, Darcian or advective fluid flow, and mobile hydrofractures. Diffusional fluid flow is the transport mechanism not necessarily involving movement of fluid. Even in a completely stagnant fluid, there can be a net flux of dissolved material

through the fluid if there is a gradient in chemical potential of that dissolved material and the fluid provides a connected pathway. Diffusion is a geologically very important transport mechanism. It is the primary transport vehicle for dissolution-precipitation creep and metamorphic reactions (Durney 1976; Raj 1982; Rutter 1983; Drury and Urai 1990). Although diffusion is a very effective transport mechanism on the small scale (<cm ~dm), it is relatively ineffective for transport over larger distances. Thus fluid flow is the only effective mechanism for transport of dissolved material over distances (>m~km) through rocks. Aqueous fluid have a very low viscosity compared to rocks and can therefore move easily and quickly. When fluid flows, it takes its solute with it. In Darcian or advective fluid flow, fluid flows down a gradient in hydraulic head through interconnected pathways. These pathways can be distinct macroscopic channels, such as fracture or the pores inside a solid permeable rock (pervasive flow). With localized or channelized flow the fluid by-passes most of the rock volume, whereas with pervasive flow the fluid comes in close contact with most of the rock (only along grain boundaries). This of course has significant implications for the chemical interaction between fluid and rock (Rye and Bradbury 1988). In mobile hydrofracture, fluid is contained as a unit in

a fracture and both fracture and fluid move at the same time and the same rate (Weertman 1971; Secor and Pollard 1975; Pollard 1977; Takada 1990). It is invoked to explain the rapid ascent of magmas, but has received relatively little attention in metamorphic hydrology or hard-rock structural geology. Transport rates in case of hydrofracturing are not determined by Darcy's law. Transport is very rapid in the order of metres per second during the movement but may be followed by possibly long periods of stagnation or other types of flow. Hydrofracture mobility is a mechanism for rapid long distance transport of fluid without much interaction with the wall rock during transport (Davies 1999, Bons 2001).

Two main causes for precipitation inside fractures can be distinguished.

Solubility is strongly temperature dependent, with a strong pressure dependency only in the low P and high T domain. PT-lines are drawn for geothermal gradients of 20, 30 and 40°C for a lithostatic pressure-depth gradient (brown, r=2.75 • 10^3 kg/m3) and a hydrostatic pressure-depth gradient (blue, r=1.0 • 10^3 kg/m3). Contours are based on the equation for silica solubility as a function of temperature and specific volume of pure water (Fournier and Potter 1982) (Fig.3-1). Specific volume values are from tabulated data in Bowers (1995) (<2 kbar) or calculated with

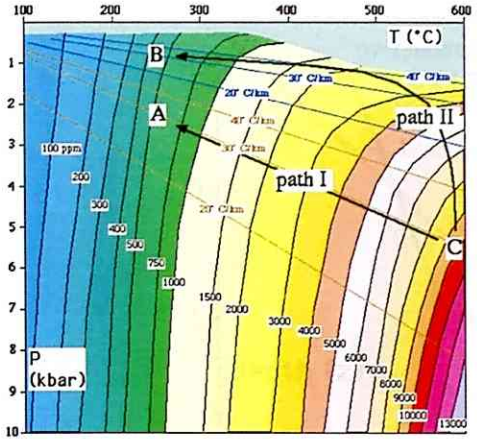

Figure.3-1 Contours of silica solubility (in ppm) in pure water as a function of pressure (P in kbar) and temperature (T in °C).

equations provided by Kerrick and Jacobs (1981) (>2 kbar). Reduction of fluid pressure (Pf) from lithostatic (point A) to hydrostatic (point B) leads to about 100 ppm (~20 %) reduction in solubility at 250 °C and a geothermal gradient of 30 °C/km. Hot metamorphic fluid (point C) has a dramatically higher solubility (~10,000 ppm). Most silica would precipitate close to the source during slow ascent (path I) (Connolly 1997). Rapid mobile hydrofracture ascent (path II) would see silica precipitation much higher in the crust.

3.2 Maximum length of a stable fluid-filled fracture

The maximum length $L_{\max}$ of a stable fracture filled with water can be estimated. The hydraulic conductivity inside an open fluid reservoir is infinite and hence the hydraulic head inside a water-filled fracture is the

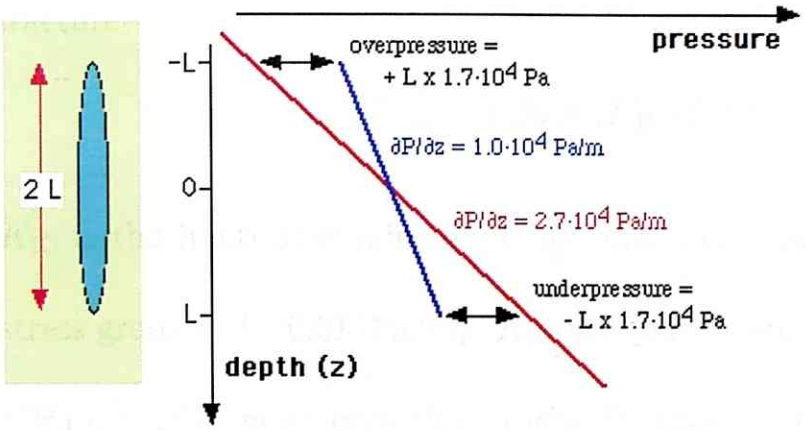

Figure.3-2 Pressure state inside a vertical fluid fracture, shown in a pressure-depth graph. The density difference between fluid and rock causes overpressure at the upper end of the fracture and underpressure at the lower end. Over- and underpressure are proportional to the length (2L) of the fracture.

same at any level in that fracture. As a consequence, the pressure inside such a fracture increases by about 10^4 Pa/m with depth. Suppose now a vertical fracture of length $2L$ filled with water in a surrounding rock with a density of 2.7×10^3 kg/m^3 and the pressure gradient about 2.7×10^4 Pa/m. It is clear that the vertical pressure gradient inside the fracture is different from that in the adjacent rock. Suppose now that the pressure balance halfway the fracture, which we take as a reference (z=0m) (Fig.3-2). At the upper tip of the fracture, the fluid pressure exceeds the rock pressure (tension) by $L\times1.7\times10^4$ Pa. The fluid is underpressured (compression) at the bottom of the fracture by the same amount of the upper tip. This puts a limit on the length of an open fluid-filled fracture. Secor and Pollard (1975) provided a simple equation to estimate the $L_{\max}$ of the vertical

fracture

$$L_{\max} = 1.36 \times (K_{\mathrm{IC}}/S)^{2/3}. \tag{3.1}$$

K_{IC} is the fracture toughness of the rock and S is the effective normal stress gradient ($\sim$0.017Pa/m). K_{IC} is about 0.1-10MPa $\mathrm{m}^{1/2}$, mostly 1-4 MPa $\mathrm{m}^{1/2}$, for intact crystalline rocks like granite, gneiss, but is probably lower for schists and low grade rocks, especially for fracturing parallel to schistosity (Atkinson and Meredith 1987). One should not that S is given here for a vertical fracture. The value of S is smaller for an inclined fracture by a factor of $\cos\theta$ than vertical (θ=0), but can be significantly higher when a fracture is subject to a tectonic stress gradient, in which case S can possibly reach values of 0.1 MPa/m. Fig.3-3 shows that vertical water-filled fractures can reach lengths of about 5-100m, most likely 10-20m. In the case of upgoing fast fluid flow into the crack supplied from large hydrothermal reservoir, hydrofracture occur and the crack grows to a few km or even to the surface until the equilibrium reachs (Nakashima 1995).

Above some critical length, the overpressure at the upper end of the fracture causes the rock to further split open, while the underpressure causes the fracture to be closed at the bottom end. If the fluid volume

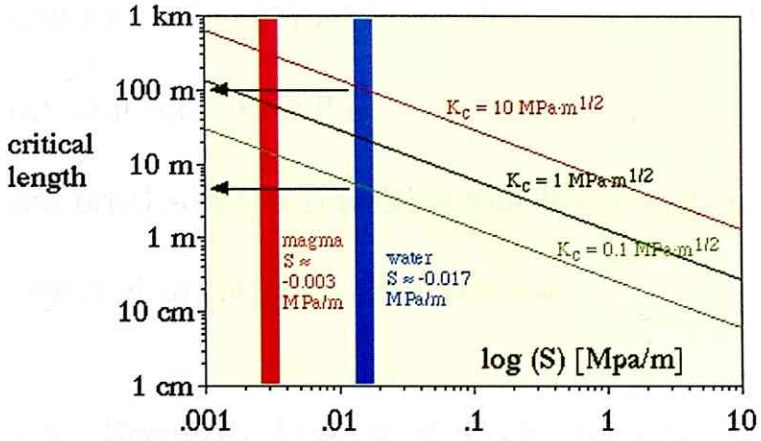

Figure.3-3 Graph of critical vertical length as a function of effective normal stress gradient (S) after Secor and Pollard (1975). For fracture toughness between 0.1 and 10 MPa m$^{1/2}$, water-filled fractures are unstable due to their buoyancy above 5 to 100m length. For comparison, granite magma-filled fractures become unstable when longer than 20 to 300m. Tectonic stress gradients can give rise to much higher S-values.

is to remain constant, opening and closure must occur in tandem and when this happens the fracture moves upwards together with its fluid in the order of metres per second. A mobile fracture can thus easily ascend through the crust in a matter of hours and stops when the conditions of (3.1) are no longer satisfied. This can be because of rock type with a higher fracture toughness encountered or when S decreases. The latter is probably the main reason for arrest. At any time it is easier for a fluid to enter pre-existing fractures than to propagate a fracture through intact rock. The presence of fractures thus causes the dispersal of fluid into these fractures, lowering S. For a hydrofracture to be mobile, the average pressure in the fluid must be lithostatic. Fluid is lost to the

wall rock when a fracture reaches lower than lithostatic fluid pressures in the wall rock. Low fluid pressures and pre-existing fractures occur above the brittle-ductile transition and hence mobile hydrofractures are to be expected to get arrested at this level.

3.3 Structural settings of the sealed-crack

The sealed-cracks of interest usually crosscut former syn-metamorphic structures and fabrics, including schistosity, folds, and earlier sealed-cracks parallel to the foliation (Fig.3-4). Most sealed-cracks are symmetrically lenticular, while a few sealed-cracks are more irregular in shape. Displacement parallel to the sealed-crack walls is mostly very small (< a few mm) or hardly observed. The geometry suggests tensile failure

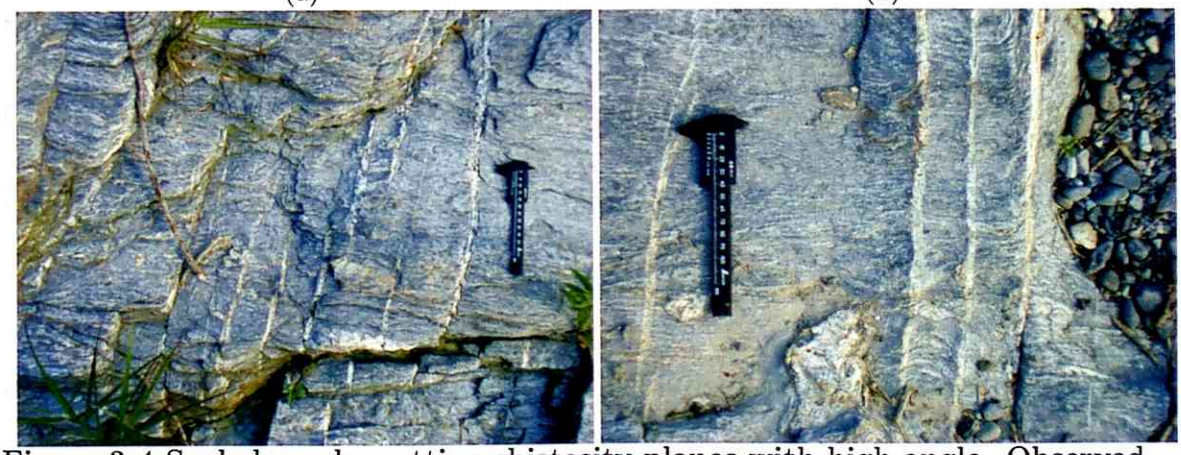

Figure.3-4 Sealed cracks cutting shistosity planes with high angle. Observed (a)obliquely upward on the schistosity planes (b)just above the schistosity planes. Location:Shiratori bridge.

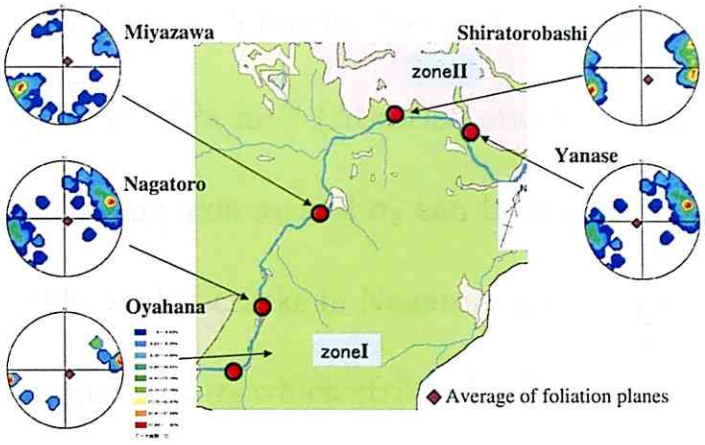

Figure.3-5 Stereographic plots (lower hemisphere) of poles to foliation and sealed-crack walls, and rose diagrams at different locations in Nagatoro area, Kanto-Mountains.

(mode I). The orientation of the sealed-crack walls, hence of the original cracks, is more or less uniform all over Nagatoro-area (Fig.3-5). The sealed-crack strike mostly north (N) to north-northwest (NNW) and dip in higher angles (60∼80° mainly) to foliations and a plumb line. Though it is not proved clearly to the direction of whether the maximum principal stress σ_1 or intermediate principal stress σ_2 the cracks grow mostly, the direction σ_1 is usually supposed to be the long axis of the cracks. According to the sub critical crack growth experiments with anisotropic granitic specimens, the fastest direction of crack growth velocity changes intermediate one to maximum one of P-wave velocity with the increase of stress intensity factor in 1∼2 MPa $m^{1/2}$ depending on humidity (water vapor pressure) and temperature (Nara 2006). As typical laboratory values of

critical stress intensity factor K_{IC} range between 1 and 4, exceptionally up to 10 MPa $m^{1/2}$ (Atkinson and Meredith 1987), both directions of the crack long axis σ_1 and σ_2 can be thought. Then the mesured orientation of the sealed-cracks in Nagatoro area is consistent with a stress field characterized by σ_3 which strikes N-NNW and dips 20° from horizontal. Most lengths and thicknesses of the sealed-cracks are measured here on the foliation plane since there are few outcrops where a vertical or near-vertical plane is exposured extensively, adding that there are little differences in measured thicknesses between the two planes in all investigattion sites.

3.4 Power-law distributions of the sealed crack

Thickness, length, and spacing of sealed cracks usually obey power-law distribution in many geologic situation (McCaffrey *et al.* 1993; Johnston 1993; Fisher *et al.* 1995; Clark *et al.* 1995; Simpson 2000; Ortega and Marrett 2000; Foxford *et al.* 2000; Laubach and Ward 2006). The power exponent D at that time shows the group feature of sealed cracks.

Thickness (aperture), length, and spacing of the sealed-cracks in pelitic schists are measured in clustered sites of the field. The field measurement of the sealed-cracks are done in the plane parallel to the host rock foliation.

Both measured length and thickness sizes of the sealed-cracks obey log-normal distributions in all sites investigated for an appropriate column interval. Log-normal distribution results generally from constant birth, proportional growth, and constant death rate in the stochastic process (Ijiri and Simon 1977; Clark 1995). Because sealed-cracks are not supposed to disappear after formation (i.e., death rate = 0), log-normal distribution is not suitable for the sealed crack formation process. On the other hand the (cumulative) size-frequency distributions of the sealed-cracks have linear parts in log-log space and thus obey power-law distributions which have an scale invariant relation between the size of an object (L) and the number (frequency) of objects of or larger than that size (N)

$$N(L) \propto L^{-D} \tag{3.2}$$

where D is the fractal dimension (Mandelbrot 1983). The larger side of the frequency distributions always converge to zero, which is a required condition for infinite energy in $D < 1$. This kind of problem are discussed in detail in a case of earthquake total moment calculation by a series of Kagan papers (Kagan 1991, Bird and Kagan 2004). Here a limit of the linearity in the larger side of the size-frequency distributions in log-log

space are assumed to be a cut-off simply. The value of D reflects the relative importance of smaller parts to larger ones, where $D > 1$ indicates that a significant portion of the extension is accommodated by the thinner and shorter sealed-crack segments in the case of their formation (Scholz and Cowie 1990, Fisher *et al.* 1995). The statistics of the sealed-cracks in the investigation sites are characterized as the D-value. The criteria in determining it is that the large amount of data should be used and the linearity hold in log-log space which is equivalent to the local maximum of the correlation coefficient between the size and the frequency. Cumulative frequency distributions of thickness and length of the sealed-cracks take power-law forms in all places. The power exponents D of thickness range 0.5-1.7 and length 0.8-1.2 respectively (Fig.3.6-3.8, Table.3-1).

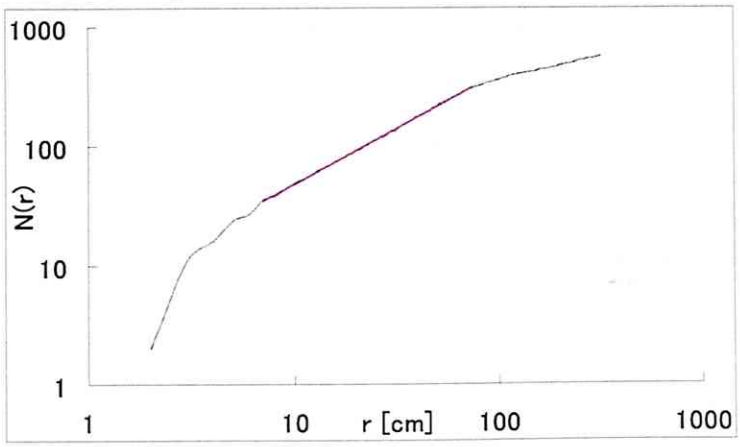

Figure.3-9 Cumulative number of two points correlation $N(r)$ vs spacing of any selected two sealed cracks (r) in the site, Miyazawa ($Dc = 0.92$) in log-log scale. The slope of the linear part (red line) gives the fractal dimension Dc in 1-D.

The fractal dimensions Dc is the relationship between the location (r) of each sealed crack and the cumulative number of two points correlation $N(r)$

$$N(r) \propto r^{Dc}. \tag{3.3}$$

If Dc is small, the degree of clustering is large. For the sealed cracks in 1-D (scan line), it ranges 0.6-1.0, but 0.7-0.9 mostly (Fig.3-9, 3-10). This results are comparable in intensity to Toriumi and Yamaguchi (2000).

Table.3-1:Parameters of the sealed crack statistics in the investigation sites.

Location	m	A.R. (L/W)	D-thickness	D-length	M.G.	N.D.[number/m^2]
Oyahanabashi	0.77	25~88	0.89(2.2-9.6)	0.77(15-80)	chlorite	1
Nagatoro(south)	0.93	125~312	0.61(2.3-10.6)	0.78(50-220)	chlorite	3
Nagatoro(north)	0.97	80~325	1.33(1.8-12)	0.87(6-19)	chlorite	6.3
Miyazawa	0.86	46~138	0.48(0.8-9.6)	0.71(10-55)	chlorite	-
Shiratoribashi	0.92	60~158	1.66(2.4-4.8)	1.13(17-90)	garnet	6.5
Yanase	0.87	110~172	1.81(2.2-4.3)	1.30(18-120)	garnet	-
Shinyashiki	1.00	21~90	1.48(4.0-15)	1.04(6.4-22.4)	biotite	(<1)
Kamigenda	1.06	15~60	0.99(1.0-11.0)	0.98(1.2-14.3)	biotite	(<1)

A.R=Aspect Ratio, M.G.=Metamorphic Grade, N.D.=Number Density

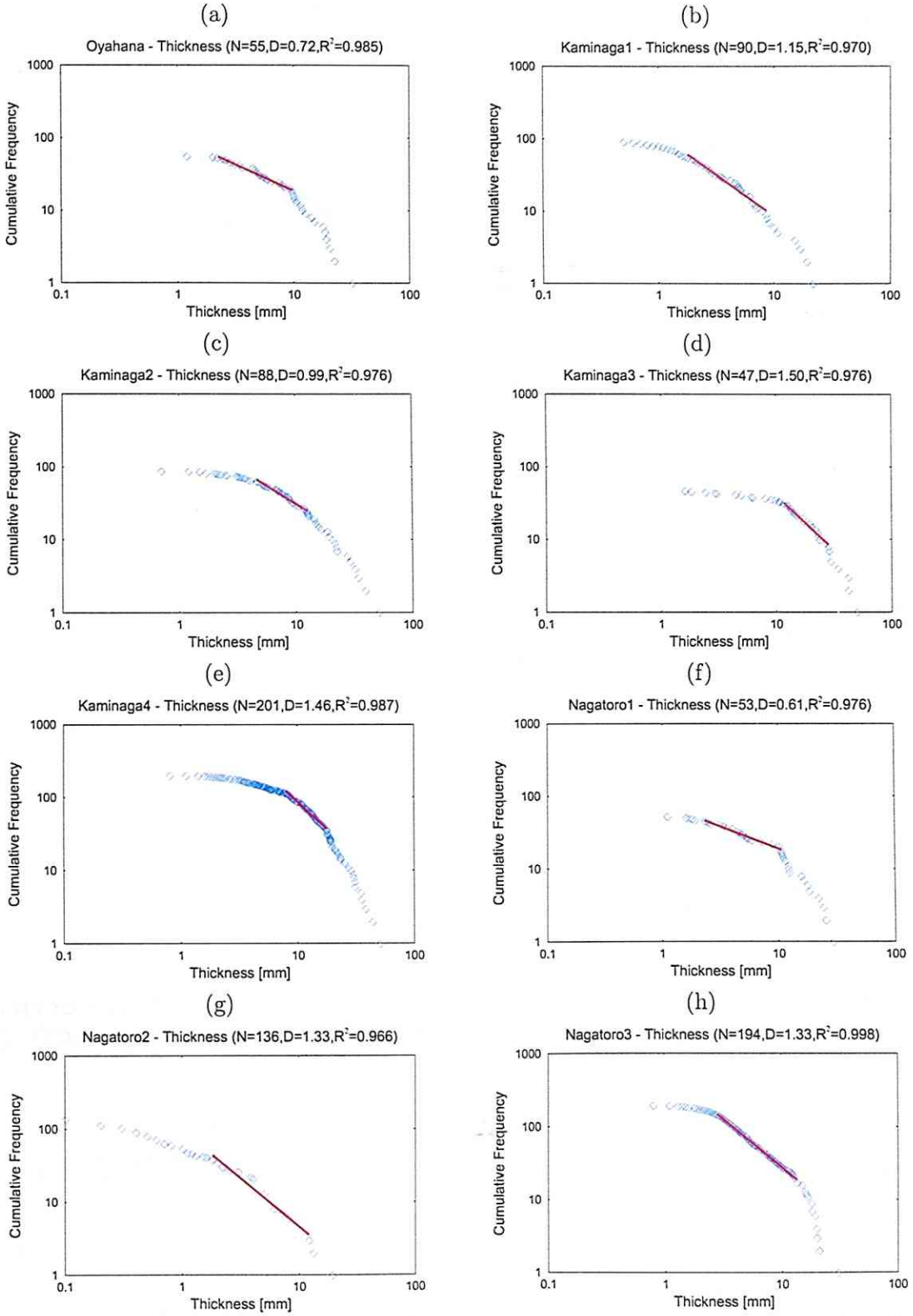

Figure.3-6 Cumulative frequency diagrams plotted in log-log space for the sealed-crack thickness in Nagatoro-area showing total number of sealed-cracks of thickness larger than T (measured normal to sealed-crack walls) versus T. Locations: (a)Oyahana (b)Kaminagatoro-1 (c)Kaminagatoro-2 (d)Kaminagatoro-3 (e)Kaminagatoro-4 (f)Nagatoro-1 (g)Nagatoro-2 (h)Nagatoro-3

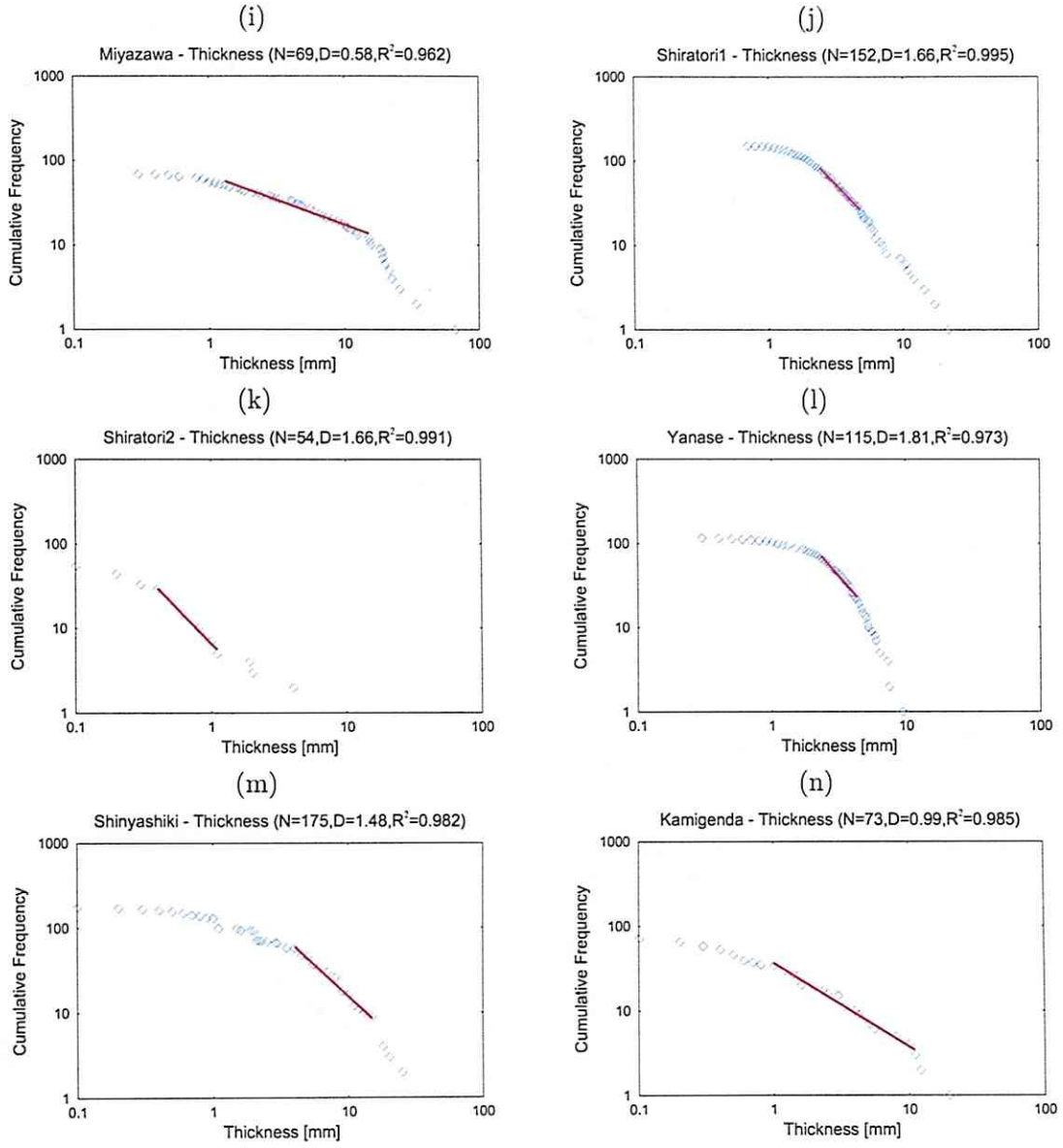

The rest of Fig.3-6 Locations: (i)Miyazawa (j)Shiratorobashi-1 (k)Shiratorobashi-2 (l)Yanase (m)Shinyashiki (n)Kamigenda

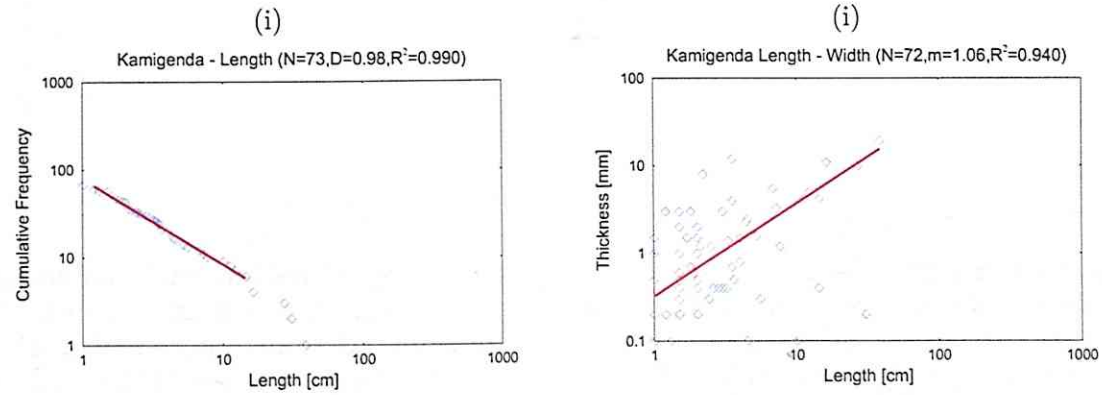

Left: The rest of Fig.3-7 (i)Kamigenda. Right: The rest of Fig.3-10 (i)Kamigenda

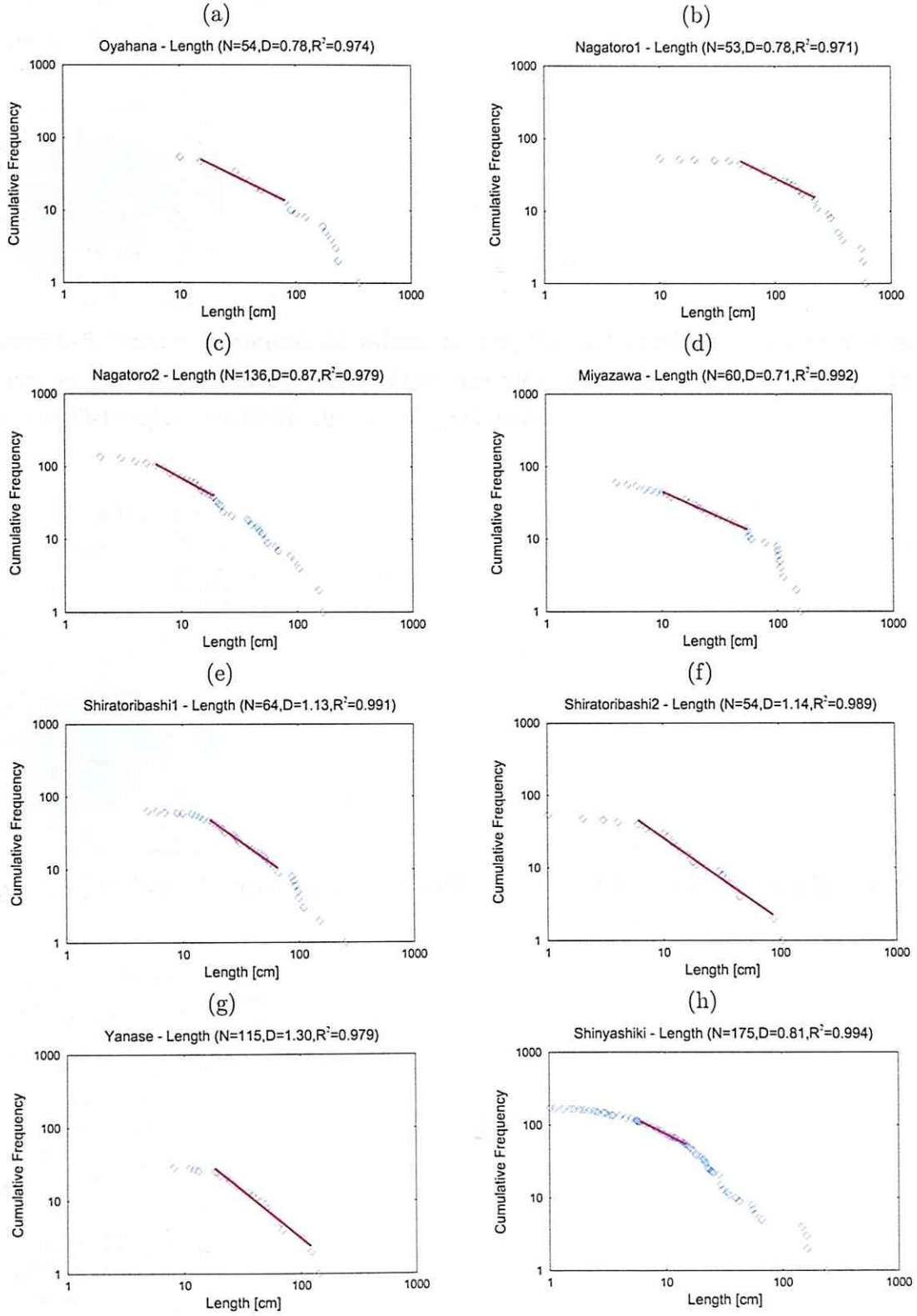

Figure.3-7 Cumulative frequency diagrams plotted in log-log space for the sealed-crack length in Nagatoro-area showing total number of sealed-cracks of length larger than L (measured parallel to sealed-crack walls) versus L. Locations: (a)Oyahana (b)Nagatoro-1 (c)Nagatoro-2 (d)Miyazawa (e)Shiratoribashi-1 (f)Shiratorobashi-2 (g)Yanase (h)Shinyashiki

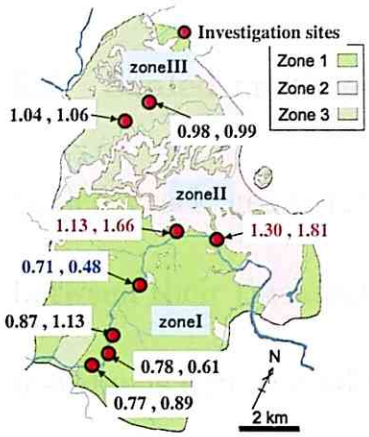

Figure.3-8 Power exponent D-values of length and thickness of the sealed cracks in the investigation sites. Left and right values within a box in each site are D-length and D-thickness respectively.

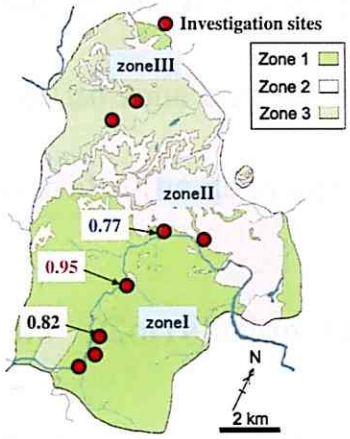

Figure.3-10 Fractal dimension Dc in 1-D (scan line) in the investigation sites.

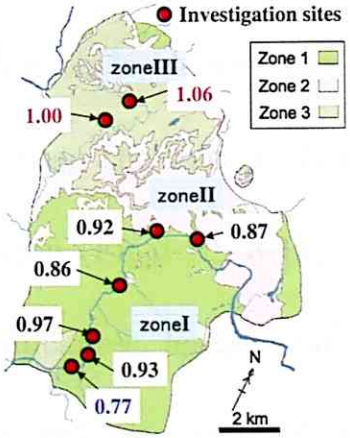

Figure.3-12 Geometrical parameter m-values estimated from the sealed cracks in the investigation sites.

3.5 Sealed crack geometry

Sealed crack geometries in all investigation sites have a good relation between their thickness and length, which holds for $W = kL^m$ (Fig.3-10). m-value is determined by the centered 50-percent data of the frequency of aspect ratio in each site, which may be a measure of the sealing process. Due to $dW/dL = kmL^{m-1}$, the growth velocity of thickness increases as length for $m > 1$ and decreases for $m < 1$. m-value is larger than 1 in biotite zone and seems to change with not only the metamorphic grade but also the degree of clustering (number density) (Table.3-1, Fig.3-12).

3.6 Correlation among the sealed crack parameters

Correlation relations among the sealed crack paramters are examind. The positive correlation of the power exponents D between thickness and length is clearly seen (Fig.3-8, 3-13(a)). The negative correlation between the fractal dimension Dc and the power exponent of size are also seen (Fig.3-10; 3-13(b)). Thus the clustering of cracks has an effect on thickness, length, and spacing simultaneously. On the other hand, there is not the significant correlation between geometrical m-value and other exponents (Fig.3-13(c)).

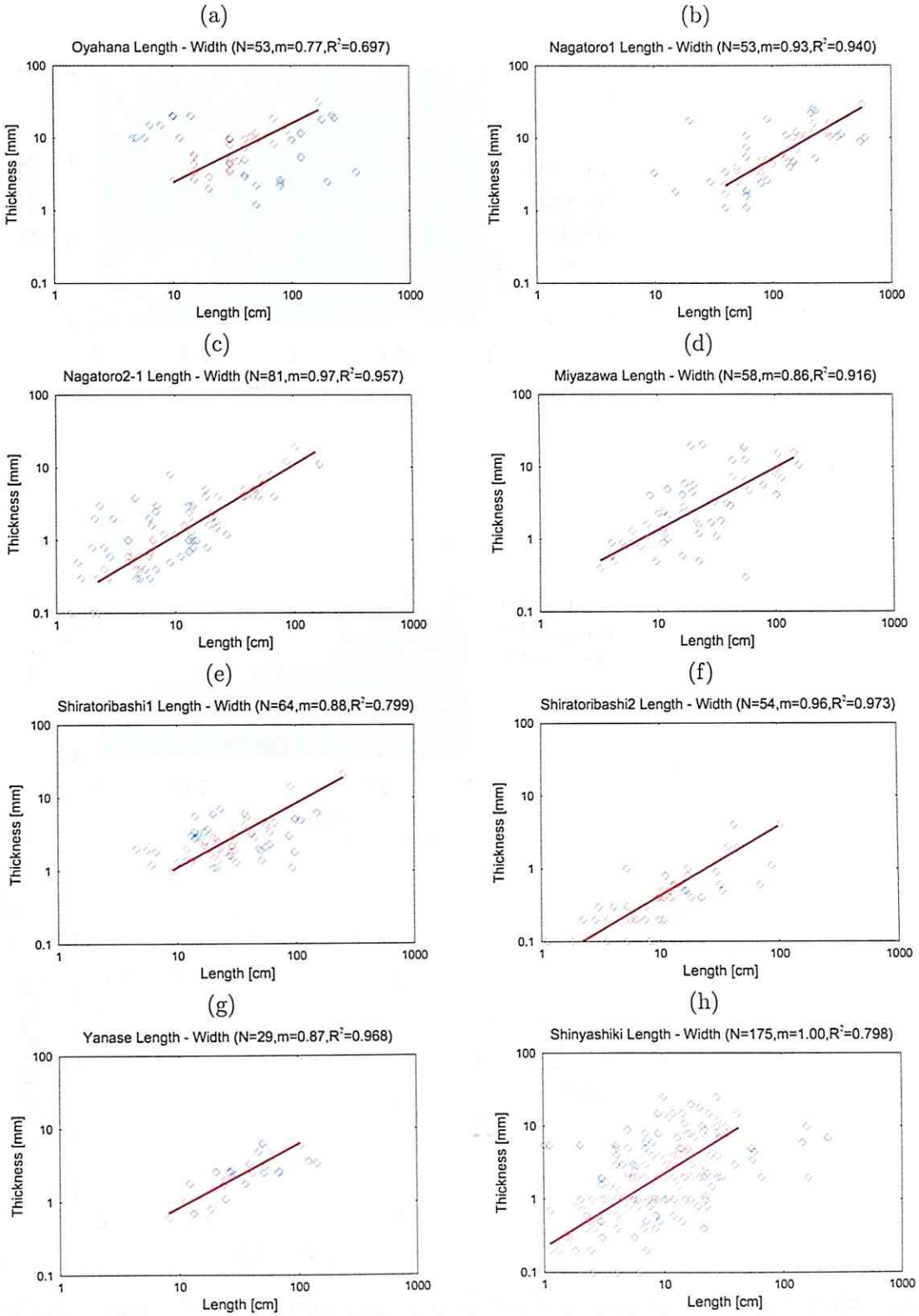

Figure.3-10 Length-thickness relation ($W = kL^m$) for the sealed cracks in each investigation site. m-value is determined by the centered 50-percent data of the frequency of aspect ratio (red line). (a)Oyahana (b)Nagatoro-1 (c)Nagatoro-2 (d)Miyazawa (e)Shiratoribashi-1 (f)Shiratorobashi-2 (g)Yanase (h)Shinyashiki

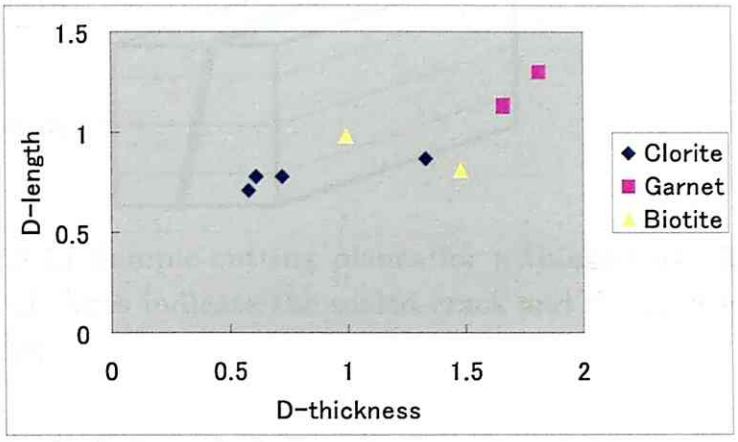

(a)

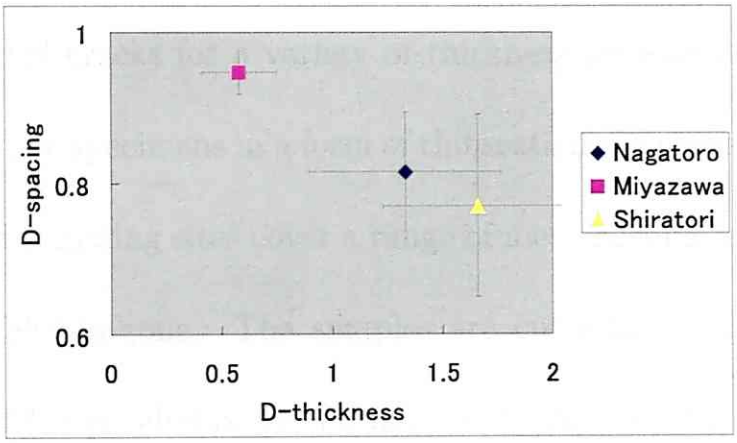

(b)

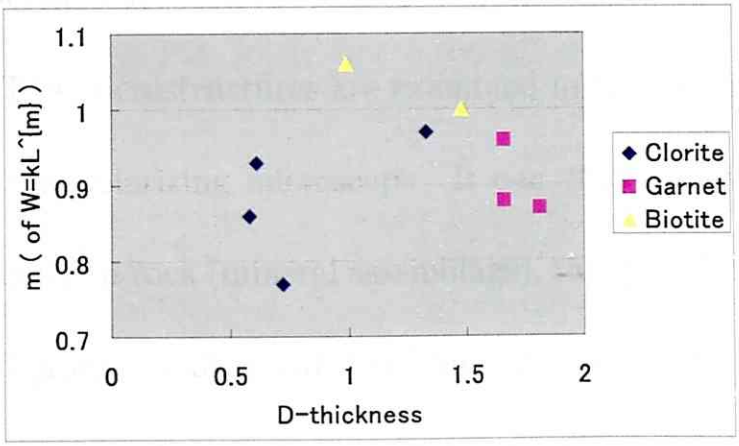

(c)

Fig.3-13 Correlations among the sealed crack parameters. (a) D-thickness and D-length. (b)D-spacing (fractal dimension in 1-D) and D-thickness. (c)D-thickness and m-value of $W = kL^{\mathrm{m}}$ (shape parameter).

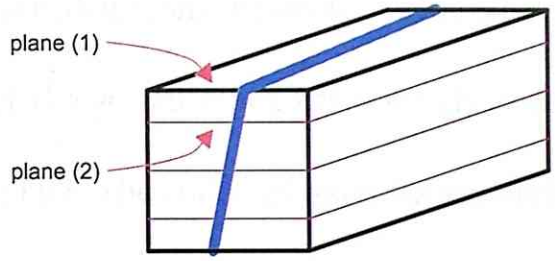

Fig.3-14 Sample-cutting planes for a thinsection. Thick blue line and thin purple lines indicate the sealed crack and the foliation or schistosity, respectively.

3.7 Fabrics of the sealed crack

Sealed cracks for a variety of thickness are sampled in the field and the sample specimens in a form of thinsection are prepared. The measurement and sampling sites cover a range of metamorphic grade from chlorite zone to biotite zone. The samples are cut normal to the sealed crack wall and (1) parallel or (2) normal to the host rock foliation (Fig.3-14). Few difference between (1) and (2) is seen below.

The microstructures are examined in thin section (about 30μm thick) with a polarizing microscope. It can elucidate which minerals are contained in a rock (mineral assemblage), the spatial arrangement, the shape, and grain-size distribution of minerals in two dimensions. Thin sections of the sealed crack forming high and low angle with the schistosity are prepared and observed through optical microscope. Mineral assemblage, width (thickness) and textures of the sealed cracks as well as host rocks are

recorded from region to region (Table.3-2-1, 3-2-2). Mineral assemblages of the sealed crack are strongly controlled by their host rock type. Host rock of the collected samples are divided into approximately 3 types; basic schist, pelitic schist and stilpnomelane schist. Details of host rock texture will be mentioned below. As shown in Table.3-2-1 and 3-2-2, the sealed cracks in pelitic schists often consist of quartz, albite, ± K-feldspar, and worm-shaped chlorite. In basic schists they often consist of calcite, chlorite, albite, ±K-feldspar, muscovite, and rutile. In stilpnomelane schists, the cracks sealed by calcite are common with few rutile and magnetite.

Four types of texture of the sealed cracks are observed. Name of the textures are following the classification by Bons(2000), namely blocky (bl), elongate blocky (eb), stretched (st) and fibrous (fb). For the observed samples, there are general tendency of constituting minerals for each texture. Blocky are composed of all minerals. In elongate blocky, albite, quartz and k-feldspar are prominent minerals and chlorite, rutile and clacite can also form. Stretched are composed of quartz, albite, k-feldspar and muscovite, and fibrous of calcite and chlorite only. Some sealed cracks show one type of texture, but others that contain more than two types of textures are common. There are two ways that the texture changes in

(a) 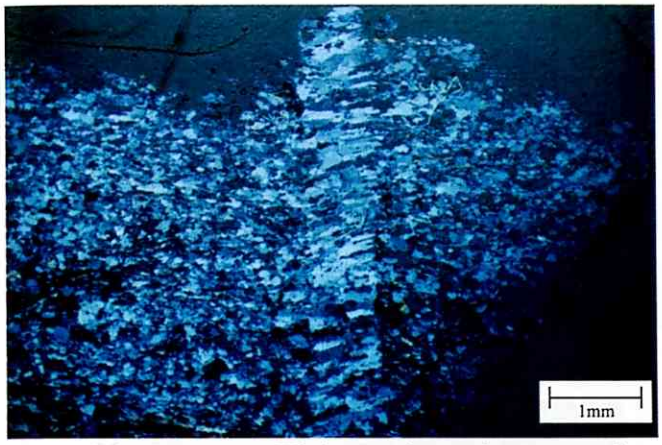

(b) 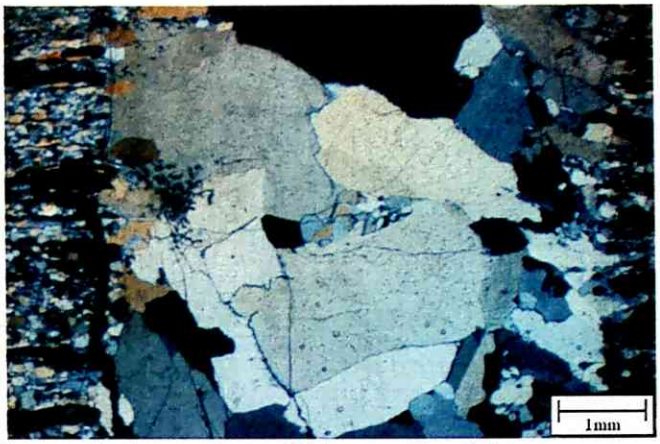

Figure.3-15 Thinsection photographs of the sealed crack at Shiratoribashi. (a)Stretched to elongate blocky texture with small thickness (<0.5mm) (open nicol) (b) Elongate blocky to blocky texture with large thickness (>6mm) (cross nicol).

a single sealed crack, i.e. along the crack wall and normal to the crack wall. Along the wall, the texture can change according to the sealed crack thickness of that point. When the sealed crack is narrow, it usually shows stretched texture (Fig.3-15(a)). As crack getting thick, texture changes from stretched to elongate blocky and finally blocky or combination of them (Fig.3-15(b)). Grain size distributions of the sealed crack can show this change with normal and log-normal distributions (Fig.3-16). Compiling the average grain sizes within the sealed crack with a variety of thickness in some locations, a linear relation between the thickness and grain long axis are clearly seen with a kink which corresponds to the texture change from stretched to elongate blocky (Fig.3-17). The kink can signifies the change of mode of material transport to the crack. For a

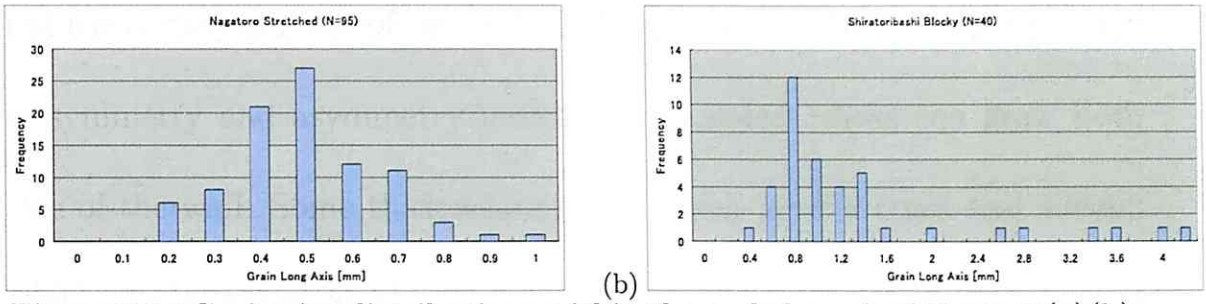

(a) (b)

Figure.3-16 Grain size distributions within the sealed crack of Fig.3-12(a)(b). (b)Log-normal distribution.

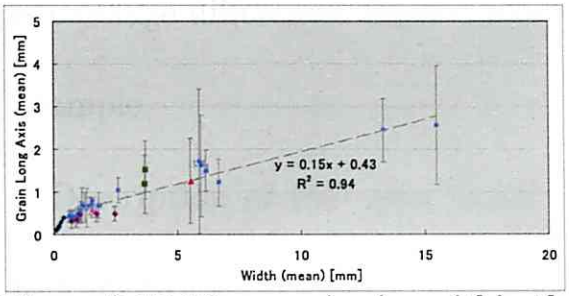

Figure.3-17 Mean grain size within the sealed crack to mean thickness there. Linear relation and a kink are clearly seen.

narrow aperture crack, diffusion from the wall rock to the crack space is possibly a dominant transport process to seal the crack. For a wide and large opening rate crack, advection can be important to transport the material for a long distance (Etheridge *et al.* 1984).

Variations of texture normal to the crack wall are often observed in thick sealed cracks. In such sealed cracks, textures are elongate blocky adjacent to the crack wall and blocky to another side of the crack. This indicates that the syntaxial crack-sealing minerals grew on the one side of the crack wall (Cox and Etheridge 1983). In some sealed cracks, the combinations of texture are symmetrical to the center line, suggesting se-

rial fracturing and seal of the crack (Okamoto *et al.* 2008). This variation of symmetry and asymmetry indicate that sealed cracks can grow both side of the wall. Some thick sealed cracks show several crack seal events, which can be recognized by the crosscutting of a few textures and mineral assemblage difference. Such changes are varying from region to region in a sample.

Description of the open (mode I) sealed crack and the host rock in each investigation site in the Kanto Mountains and Shikoku district are mentioned here.

Shiratoribashi: Host rocks are pelitic schist, which consist of quartz, albite, muscovite and chlorite with few amount of sphene, rutile and calcite. They are distributed into two types of compositional banding, qtz-rich layer (quartz, albite, calcite and chlorite) and Mus-rich layer (muscovite chlorite, albite, sphene and rutile). Qtz-rich layers can be divided into fine layers and coarse layers. Grain sizes of quartz and albite are approximately 100μm for fine layer and 30μm for coarse layer. Open sealed cracks cut across these bands. Thickness of them are 500μm-1000μm. Open cracks are consists of quartz, albite and chlorite ($\pm$ k-feldspar, calcite). Texture of them varies from stretched to elongate blocky. Some

quartz and albite contain vermicular (worm-shaped) chlorite. No texture cuts other textures, which indicates no significant change in the mechanism of crystal growth during sealed crack formation.

Kaminagatoro: Host rocks are banding pelitic schist and stilpnomelane schist. Grain sizes of pelitic schist are smaller than that of Nagatoro area, around 50μm for quartz, 20μm for muscovite, 30μm for rutile. Open sealed cracks of pelitic schist consist of quartz and k-feldspar. Their thickness is 350-1500μm. Their textures vary from elongate blocky to blocky. Asymmetric textures of sealed crack are observed where elongated blocky crystals of one side of the crack wall are larger than that of the other side. That indicates that crystal growth from one side of the vein was faster than that of the other. Again, no multiple texture are observed. Stilpnomelane schist is composed of quartz, albite, stilpnomelane, pyrite magnetite and rutile. The boundary between pelitic schists is sharp. Open sealed cracks in stilpnomelane schist cut schistosity, but don't often extend into adjacent pelitic schist. The sealed cracks are composed of calcite some times accompanied with rutile. Calcite shows a fibrous texture and rutile grows from host rock rutile (stretched) (Fig.3-18).

Nagatoro: Host rocks are also banding pelitic schist with quartz grain

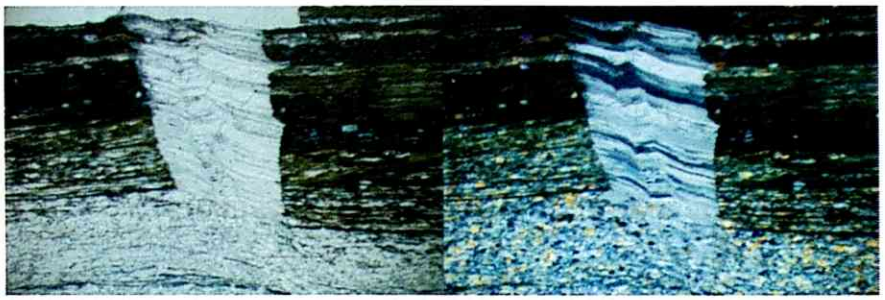

Figure.3-18 Thinsection photograph of fibrous calcite sealed cracks with 1.25mm thickness in stilpnomelane schist, Kaminagatoro (left: open nicol, right: cross nicol) (Thinsection 1-2).

size of around 100μm. Thicknesses of the sealed cracks are fairly large ranging from 600μm-12400μm. They consist of quartz, albite, k-feldspar, vermicular chlorite. The textures of the sealed cracks vary from stretched to elongate blocky and blocky. Thick sealed cracks (>2000μm) show textures of elongate blocky near crack wall and blocky in the center of the crack. As shown above, some sealed cracks contain both stretched and elongate blocky texture, which indicates the change of crystal growth mechanism during crack formation.

Kokuryo-river in central Shikoku within garnet zone: Host rocks collected here are banding pelitic schist consisting of quartz, muscovite, albite, and sphene ($\pm$ garnet and epidote). Open sealed cracks are composed of quartz, albite and sometimes small amount of vermicular chlorite in quartz. Their thicknesses are 220μm-3600μm with textures ranging from stretched to elongate blocky and blocky. For thickness less than 1000μm,

a combination of stretched and elongate blocky texture is common. The texture changes not along the crack wall, but normal to it. On the other hand, in thickness more than 1000μm, a combination of elongate blocky and blocky texture is observed. The texture changes normal to the crack wall. No texture cuts across others. Samples of shear sealed cracks (mode II or III) are also collected and observed. The mineral assemblage and the texture of the shear sealed crack are fairy different from open sealed cracks. The mineral assemblages of shear sealed cracks are quartz, albite and sometimes accompanied with muscovite, calcite and epidote. Quartz and albite usually shows interfingered boundary. Muscovite grows among the grain boundary of quartz or albite. Grains of quartz and albite are elongated and their long axes are parallel to the schistosity. The shape of them are wide parallel to the shistosity, which may mean a shear sliding on the plane.

Outcrops along the coast: Host rocks are basic schist composed of albite, chlorite, epidote, actinolite and rutile. Mineral assemblage in the open sealed cracks is fairly different from that in pelitic schist. Chlorite and albite are main and $\pm$ k-feldspar, calcite, muscovite and rutile are a little. Sealed crack thicknesses range from 240μm to 16000μm. Those with

(a) 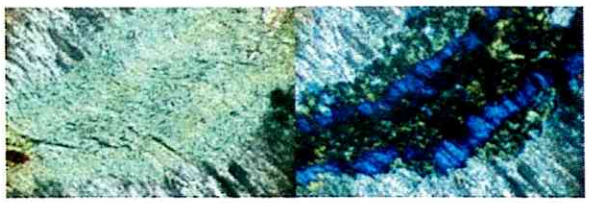 (b) 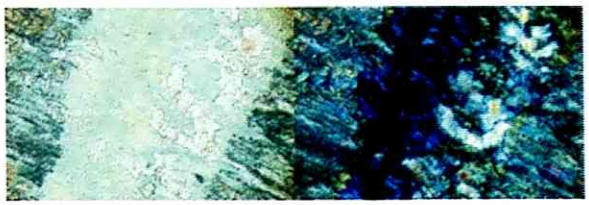

Figure.3-19 Multiple textures seen with in a same crack (open and cross nicol). (a)fibrous chlorite (b)Elongate blocky chlorite and albite.

a thickness more than 1000μm contain calcite layer cutting pre-existin texture, whereas less than 1000μm don't. fibrous chlorite cuts elongate albite+chlorite, but is cut by blocky chlorite+albite+rutile. Sealed cracks with only fibrous chlorite, blocky chlorite+albite+rutile, or elongate albite+chlorite are also observed. This implies that there were a number of crack and seal events with different crystal growth rate in this region within the same crack.

The scanning electron microscope (SEM)-based technique of electron probe micro-analysis (EPMA) using polished thin sections yields microstructural information with a resolution on the micrometre scale and provides information on the spatial distribution of the components (contour map of components in two dimensions) and the quantitative composition of the minerals within a beam radius by comparing the spectroscopy for characteristic X-ray with standard samples.

Chemical composition of some minerals in the sealed crack are different

from that in the adjacent wall rock with specific elements of the mineral. Ca component of albite and Mn of chlorite are usually higher than the wall rock, which is indicative of external high-P,T rapid and advective fluid flow into the crack (Fig.3-20). Some albites show significant component stripes in a sealed crack parallel to the wall, which seems to reflect several times of fracturing and following sealing in the same crack in accordance with the textural observation above. In the wall rock adjacent to such albite or worm chlorite, significant depletion zone can not be seen. Consequently by the facts, positive feed back mechanism of fluid flow and the fluid-filled crack are suggested naturally.

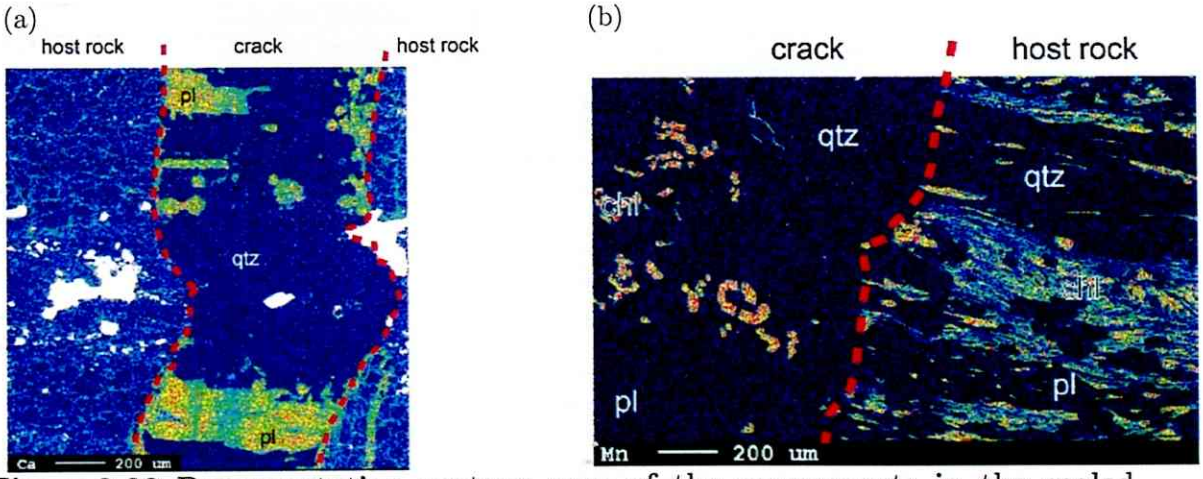

Figure.3-20 Representative contour map of the components in the sealed crack. (a)High-Ca component albeit with stripes parallel to the crack wall. (b)High-Mn component worm chrolite.

Table.3-2-1 Mineral assemblage of the sealed crack and host host rock in each thinsection.

Thinsection No.	Location	Type	Texture	Thickness [mm]	Host rock type
1-2	Kaminagatoro	open	fb	1.25	stilpnomelane
1-3				0.05	
				0.14	
				0.08	
1-6	Nagatoro	open	st	0.23	pelitic
				0.33	
				0.28	
				0.48	
1-8	Shiratori bridge	open	bl	5.4	pelitic
1-10	Nagatoro	open	st	0.85	pelitic
1-11			bl	6.8	
1-14	Kaminagatoro	shear	bl(wavy ex.)	0.65	basic
1-16	Nagatoro north	open	multi	16	basic
			(eb)	4.5	
			(layer)	7.2	
			(eb)	0.8	
			(layer)	3.2	
			(eb)	0.8	
1-20	Miyazawa	open	eb	8	pelitic
1-23			multi	>10	
1-26	Kameiwa(Shikoku)	open	eb	5.6	pelitic
2-1	Shiratori bridge	open	eb	1.0	pelitic
				0.5	
2-2			eb+bl	1.1	
2-4		shear	bl	3	
2-7	Kaminagatoro	open	bl	1.5	pelitic
2-8			st	0.4	
2-9	Nagatoro	open	eb+bl	18	pelitic
2-10			eb+bl	7.2	
			st	0.5	
2-11			eb+bl	8.0	
2-12			eb	3.6	
2-13			eb+bl	9.5	
			eb	2.5	
			eb+bl	4.5	
2-14			multi	13.4	
			(eb)	3.2	
			(eb)	3.2	
			(bl)	5.0	
			(eb)	1.0	
			(eb)	1.0	

Table.3-2-1

Sealed crack minerals									Host rock minerals									
Qtz	Ab	K-f	Chl	Chl(worm)	Cal	Mus	Epi	Rt	Qtz	Ab	Mus	Chl	Grt	Epi	Act	Sph	Rt	Cal
					+				+	+								
					+			+	+	+								
					+			+	+	+								
					+				+	+								
+											+							
+											+							
+											+							
+				+							+							
+	+				+				+	+	+	+						
+	+	+							+	+	+	+						
+	+			+					+	+	+	+						
+	+				+				+	+		+		+				
	+			+	+				+	+		+		+				
	+			+					+	+		+		+				
					+				+	+		+		+				
	+			+					+	+		+		+				
					+				+	+		+		+				
	+				+				+	+	+							
+	+				+				+	+	+							
+	+								+	+	+							
+				+	+				+	+	+	+				+	+	+
+		+		+					+	+	+	+				+	+	+
+	+			+					+	+	+	+						
+	+				+				+	+	+							
+		+			+				+	+	+						+	
+		+			+				+	+	+						+	
+	+			+					+		+						+	
+	+	+		+					+		+							
+									+		+							
+	+								+		+							
+	+	+							+		+							
+	+	+							+		+							
+	+	+		+					+		+							
+	+			+					+		+		+					
+									+		+		+					
	+								+		+		+					
+				+					+		+		+					
	+								+		+		+					
+									+		+		+					

Table.3-2-2 Mineral assemblage of the sealed crack and host host rock in each thinsection.

Thinsection No.	Location	Type	Texture	Thickness [mm]	Host rock type
2-15	Nagatoro	open	eb+bl	>10	pelitic
			st	0.9	
			st	0.6	
			eb+bl	5.6	
			eb+bl	3.6	
			st	0.8	
2-17			eb+bl	7.2	
2-19	Kokuryo river (Shikoku)	shear	bl(wavy ex.)	2.5	pelitic
2-21				7.2	
2-23				2.2	
2-24				1.4	
2-27		open	eb+bl	3.0	
2-28			eb	1.0	
2-29			eb+bl	3.6	
			st	0.35	
			eb	1.8	
2-31	Outcrops along the coast (Shikoku)	shear	bl(wavy ex.)	9.6	basic
2-38		open	multi	16	
			(eb)	3.2	
			(layer)	5.0	
			(eb)	2.0	
			(layer)	2.0	
			(eb)	4.0	
2-39			multi	16	
			(eb)	2.8	
			(layer)	1.0	
			(eb)	1.2	
			(layer)	3.0	
			(eb)	2.5	
			(eb)	3.0	
2-40			eb	0.95	
			st	0.24	
			multi	0.85	
			(st)	0.22	
			(st)	0.20	
			(st)	0.18	
			(st)	0.10	
			(st)	0.15	
2-43			eb	1.0	

Table.3-2-2

Sealed crack minerals									Host rock minerals									
Qtz	Ab	K-f	Chl	Chl(worm)	Cal	Mus	Epi	Rt	Qtz	Ab	Mus	Chl	Grt	Epi	Act	Sph	Rt	Cal
+	+			+					+		+							
+									+		+							
+									+		+							
+				+					+		+							
+	+								+		+							
+									+		+							
+	+			+					+	+	+							
+	+					+			+	+	+	+	+	+				
+	+									+		+						
+	+					+				+		+	+	+				
+	+					+				+		+	+	+				
+	+								+	+	+					+		
+	+								+	+	+					+		
+	+			+					+	+	+	+				+	+	
+									+	+	+	+				+	+	
+	+								+	+	+	+				+	+	
+					+					+		+		+	+		+	
	+		+		+					+		+		+	+			
	+		+							+		+		+	+			
					+					+		+		+	+			
	+									+		+		+	+			
					+					+		+		+	+			
	+		+							+		+		+	+			
	+		+		+					+		+		+	+			
					+					+		+		+	+			
	+				+					+		+		+	+			
	+				+					+		+		+	+			
	+				+					+		+		+	+			
	+				+					+		+		+	+			
	+	+	+					+		+	+	+		+	+			
			+					+		+	+	+		+	+			
	+	+	+			+		+		+	+	+		+	+			
	+	+	+							+	+	+		+	+			
			+			+				+	+	+		+	+			
	+		+					+		+	+	+		+	+			
			+							+	+	+		+	+			
	+	+	+							+	+	+		+	+			
	+		+							+	+	+		+	+	+	+	

4 Models and discussions

4.1 Mixed-mode fracture

Strike and dip of the sealed cracks which come clearly from the tensional fracture should record the direction of crack initiation because stress intensity factor increases with the crack growth and the next fracture should occur from the tip of the crack. Angles between the sealed cracks and the shistosities are distributed mainly around 70° in all investigation sites and can be associated with the mixed mode fracture where open tensional cracks (mode I) and shear faulting cracks (mode II or III) are formed simultaneously in passing with pressure solutions on the dipole stress field around a pure shear faulting plane. Many workers have suggested that sealed cracks initiate from cavity formation with ductile shear deformation (Vermilye and Scholz 1995; Olson 2003; Nüchter and Stöckhert 2007) and grow as a repetitious open mode fracture followed by a sealing of minerals from external hydrothermal fluid transported as advection with enhanced permeability through the fractured rock. (Etheridge *et al.* 1984). Here is assumed that the rock mass is treated as a linear elastic body, the schistosity planes are the weak plane for faulting, and mode III component of

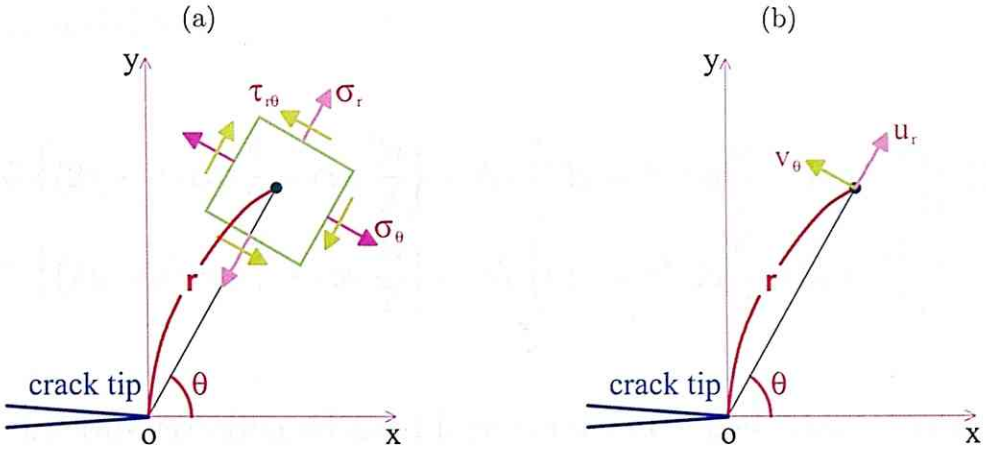

Fig.4.1 Stress and displacement component in polar coordinates. (a)Stress (b)Displacement.

the shear displacement can be negligible. Stresses around a crack under plain strain and mode I, II condition in circular cylindrical coordinates is given by a transformation from Cartesian coordinates and superposition of each mode (Fig.4.1)

$$\sigma_r = \frac{1}{\sqrt{2\pi r}} \frac{1}{2} \left\{ K_{\mathrm{I}}(3 - \cos\theta)\cos\frac{\theta}{2} + K_{\mathrm{II}}(3\cos\theta - 1)\sin\frac{\theta}{2} \right\} \quad (4.1)$$

$$\sigma_\theta = \frac{1}{\sqrt{2\pi r}} \frac{1}{2} \left\{ K_{\mathrm{I}}(1 + \cos\theta)\cos\frac{\theta}{2} - K_{\mathrm{II}} 3\sin\theta\cos\frac{\theta}{2} \right\} \quad (4.2)$$

$$\tau_{r\theta} = \frac{1}{\sqrt{2\pi r}} \frac{1}{2} \left\{ K_{\mathrm{I}}\sin\theta\cos\frac{\theta}{2} + K_{\mathrm{II}}(3\cos\theta - 1)\cos\frac{\theta}{2} \right\} \quad (4.3)$$

$$\sigma_z = \nu(\sigma_r + \sigma_\theta) \quad (4.4)$$

where ν is Poisson's ratio and $K_{\mathrm{I}}, K_{\mathrm{II}}$ are stress intensity factors in each mode respectively described below. Displacement fields are given similarly

by shear modulus μ

$$u_r = \frac{1}{4\mu}\sqrt{\frac{r}{2\pi}}\left[K_{\mathrm{I}}\left\{(2\chi-1)\cos\frac{\theta}{2}-\cos\frac{3\theta}{2}\right\}-K_{\mathrm{II}}\left\{(2\chi-1)\sin\frac{\theta}{2}-3\sin\frac{3\theta}{2}\right\}\right] \quad (4.5)$$

$$v_\theta = \frac{1}{4\mu}\sqrt{\frac{r}{2\pi}}\left[K_{\mathrm{I}}\left\{(2\chi-1)\cos\frac{\theta}{2}-\cos\frac{3\theta}{2}\right\}-K_{\mathrm{II}}\left\{(2\chi-1)\sin\frac{\theta}{2}-3\sin\frac{3\theta}{2}\right\}\right]. \quad (4.6)$$

The fracture criterion adopted here is the circumferential stress maximum one proposed by Erdogan and Sih (1963) that the tensional fracture (mode I) accompanying shear displacement (mode II) is assumed to occur to the direction where the circumferential stress intensity factor K_σ near the shear crack tip is maximized and reaches K_{IC} with the angle θ_c

$$\begin{aligned} K_{\sigma\max} &= \sigma_{\theta\max}\sqrt{2\pi r} \\ &= \frac{1}{2}\left\{K_{\mathrm{I}}(1+\cos\theta_c)\cos\frac{\theta_c}{2}-3K_{\mathrm{II}}\sin\theta_c\cos\frac{\theta_c}{2}\right\} = K_{\mathrm{IC}} \end{aligned} \quad (4.7)$$

which is widely used because this is easy to understand and capable of explaining the experimental data. As examples of other representative criterion, the strain energy density criterion and the energy release rate maximum criterion are pointed. Their prediction of the initial direction of mixed mode fracture doesn't differ much from the circumferential stress maximum criterion adopted here.

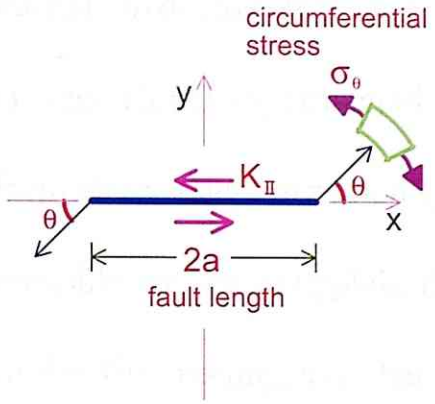

Fig.4-2 Idealized diagram of a small fault represented as a mod II crack. The circumferential stress σ_θ acting on the element near the crack tip is shown in polar coordinate system.

Same kind of analysis is done by Ripsoli (1981) who investigated a number of veins and pressure solution surfaces which emanate from near the ends of small left-lateral faults. The structures are found in an outcrop of limestone in the Languedoc region of southern France. The tectonic setting and details of the small scale structures are described by him who hypothesize that stress concentrations resulting from slip on the small faults caused the veins and solution surfaces to form and propagate away from the fault terminations. It shall be demonstrated that the situation are consistent with his hypothesis, except right-lateral is feasible for the sealed cracks here.

The main conditions of note in many cracks with fluid are high fluid (pore) pressure and low effective normal stress locally. In such a sit-

uation, hydrofracture may be effective to cause the tensional (mode I) cracks. But if so, principal stress σ_1 are inclined stably about 20° away from the vertical direction (z) during the exhumation stage of the metamorphic terrain to explain the strike-dip distribution of the sealed cracks under the assumption that the schistosity plane are nearly horizontal. Although it is probable in the subducting plate region, the seal and compartment structure or strength inhomogeneity with permeability contrast are more desirable for hydrofracture and the spatial sealed crack pattern in long scale are dominated by the pre-existing structure (Nakashima 1995). This idea is less predictive for the events to come unless the structure are known, where also strike and dip of a crack are too sensitive to σ_1 which might vary the direction with time and space. The result that the strikes and dips of the sealed crack obeys the same distribution in all investigation sites may require the model that the initiative direction of the crack doesn't depend much on effective σ_1 reduced by high fluid pressure. The mixed mode fracture model with the shear displacement along the weak schistosity planes enables it and simultaneously a fat shape (discordant) sealed cracks increasing apparent fracture toughness K_{IC}^* much greater than the values for K_{IC} in the laboratory (Atkinson and Meredith 1987,

Nüchter and Stöckhert 2007).

Linear elastic fracture mechanics (LEFM) predicts that the aperture w of an arrested crack correlates with the crack length L and with the wall normal effective tensile stress $\sigma'_{\mathrm{n}} = \sigma_{\mathrm{n}} - P_{\mathrm{f}}$. The following relation holds for non-interacting, opening mode cracks under two-dimensional plane strain conditions (Pollard and Segall 1987)

$$w = -\sigma'_{\mathrm{n}} \frac{2(1-\nu^2)}{E} L \tag{4.8}$$

where E denotes the Young's modulus and ν the Poisson's ratio. The state of stress in the material close to the tip of a crack at a distance r under tensile load is proportional to the stress intensity factor K_{I} and $r^{-1/2}$. The stress intensity factor K_{I} depends on σ'_n and on L

$$K_{\mathrm{I}} = -\sigma'_{\mathrm{n}} \sqrt{\pi \frac{L}{2}} \tag{4.9}$$

which is same form for K_{II} or K_{III} with the change of σ'_{n} to corresponding shear stress σ_{II} or σ_{III}. If K_{I} reaches a certain material constant, the fracture toughness K_{IC}, the material fails by initiation of unstable crack

propagation

$$K_{IC} = -\sigma'_{nc}\sqrt{\pi\frac{L}{2}} \tag{4.10}$$

where σ_{nc} denotes the critical tensile stress under the constant crack length L (or L_{max} in (3.1)). According to (4.8)-(4.10) crack opening by linear elastic distortion of the host rock is limited by $\sigma'_n < \sigma'_{nc}$. Implementation of (4.10) into (4.8) yields a criterion for the maximum possible crack width w_0 sustained by the host rock (Olson 2003)

$$w_0 = K_{IC}\frac{1-\nu^2}{E\sqrt{\pi/8}}\sqrt{L}. \tag{4.11}$$

(4.11) solved for K_{IC}

$$K_{IC} = \frac{w_0}{\sqrt{L}}\frac{E\sqrt{\pi/8}}{1-\nu^2} \tag{4.12}$$

can be used to estimate K_{IC} holding for the rock using the length and aperture data of sealed cracks. This approach presumes that cracks formed in response to purely elastic distortion of the host rock and under LEFM-conditions. (4.12) is also used to compare the geometry of the discordant sealed cracks to laboratory data for K_{IC}. These include veins at Culpepper Quarry (Virginia USA, upper Triassic) where excellent bedding plane exposure of calcareouly cemented Balls Bluff Siltsone contains

several calcite-filled vein sets, and Florence Lake (California USA) where spectacular exposures of glacially polished Mount Givens Granodiorite are cut by a set of steeply dipping chlorite- and epidote-filled fractures, as well as multi-segment dykes at Ship Rock (Vermilye and Sholtz 1995; Delaney and Pollard 1981). The geometry of the Culpepper Quarry and Florence Lake veins is interpreted to result from elastic distortion of the vein walls during cavity formation accompanied with shear deformation. In contast, the geometry of magmatic dykes is expected to be strongly influenced by thermal effects due to magmatic heat transfer. Such effects include thermal erosion at the dyke walls and enhanced plasticity at the dyke tips, resulting in a marked increase in the fracture toughness K_{IC} due to crack tip blunting. The geometry of magmatic dykes is expected to be influenced by a number of processes and does hardly reflect a purely elastic deformation of the host rock. The Sambagawa metamorphic rock also have been reported to record plastic deformation in several stages which include post metamorphic exhumation (). Thus it is easily conceivable that shear deformation had affected the rock in crack formation followed by mineral sealing assisted by hydrothermal fluid due to thermal inertia of the rock to the temperature range of brittle-ductile transition.

As K_{IC} is exclusively defined for sharp crack tips stressed at LEFM-conditions, the predictions based on (4.12) are referred to as apparent fracture toughness K^*_{IC} much greater than K_{IC} in the laboratory. (4.12) is estimated for the length and thickness data of the sealed cracks in some locations in the Sanbagawa metamorphic terrain using moderate values of E=50 GPa and ν=0.25 for memamorphic rocks (Turcotte and Schubert 2002). The resulting K^*_{IC} values of the sealed crack within the Sanbagawa metamorphic rock are 50~2000 MPa $m^{1/2}$ but mostly 100~1000 MPa $m^{1/2}$ with a tendency that the value is prone to be large (fat shape) in high grade area. This is larger than 8~25 MPa $m^{1/2}$ of the mineralized veins in Culpepper Quarry and Florence Lake but slightly smaller than 300~3000 of the Styra-Ochi Unit in Southern Evia Island, Greece, which is part of the high pressure and low temperature (HP/LT) metamorphic internal Cyclades belt situated in the backarc region of the active Hellenic subduction zone (Nüchter and Stöckhert 2007 and its references) and is interpreted to show the degree of deformation of the rock. The value K^*_{IC} is one of the geometrical parameter and thought an alternative of the m-value of w=kL^m. Thus it is reasonable that the two geometrical parameters indicate a similar tendency.

In the analysis for the mixed mode fracture, let the x_1 axis be parallel to the left lateral fault trace, x_2 axis be normal to the fault, and r, θ be as polar coordinate (Fig.4-2). For simplicity, K_{I} is assumed here as zero, proper for σ_1 inclined 45° from vertical. Although it is not correct, the schistosity planes are imaginably weak for the shear strength, thus sensitive to shear stress, and greases shear motion (mode II or III). In order to find the planes which carry the maximum and minimum circumferential stress to the mode I fracture near the mode II crack tip, (6.2) is differentiated with respect to θ and the result is set to zero with the angle θ_c

$$\cos(\theta_c)\cos(\frac{\theta_c}{2}) - \frac{1}{2}\sin(\theta_c)\sin(\frac{\theta_c}{2}) = 0 \tag{4.13}$$

which is satisfied for the left lateral fault if $\theta_c \approx 70.5°$ for the opening crack (maximum tensional circumferential stress) and $\theta_a \approx -70.5°$ for the anti-crack or pressure solution (maximum compressional circumferential stress). This is comparable to the measured result of the sealed cracks regarding the schistosity plane as faulting shear plane (Fig.4-3).

The criteria (4.7) and (4.13) enables an estimation of the corresponding K_{II} falut length Ls

$$\mathrm{Ls} = \frac{1}{\pi}\left[\frac{2K^*_{\mathrm{IC}}}{3\sigma_{\mathrm{II}}\sin(\theta_c)\cos(\theta_c/2)}\right]^2 \tag{4.14}$$

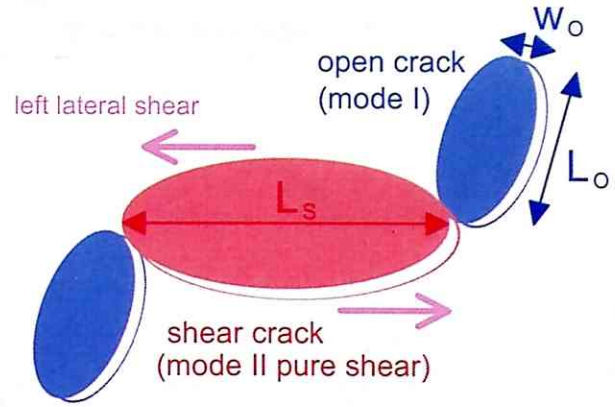

Fig.4-3 Illustration on the mixed mode cracks making new surfaces.

under the assumptions; (1) mode II shear stress σ_{II} is 50 MPa derived from the differential stress of about 100 to 150 MPa for the chlorite to oligoclase-biotite zone (Toriumi 1978; Toriumi *et al.* 1984; Toriumi *et al.* 1986; Toriumi 1990). (2)θ_c is the angle between the mode I crack and the envisaged fault (schistosity). If no data, a substitute 70°, the measured main value, is used for simplicity. (3)One sealed cracks corresponds to one fault (a pair of planes). Hence the model gives the fault length distribution in each site, which is known to take a power-law form (Scholz and Cowie 1990). The power exponent Df of the estimated fault length by the application of the sealed crack data to the model is proportionally related to b-value of earthquake statistics (Fig.4-4). Df is greater than in zone II (garnet zone) than other zones except Oyahana (zone I) affected by the scarce strike-dip data of the sealed crack. The tendency of Df is

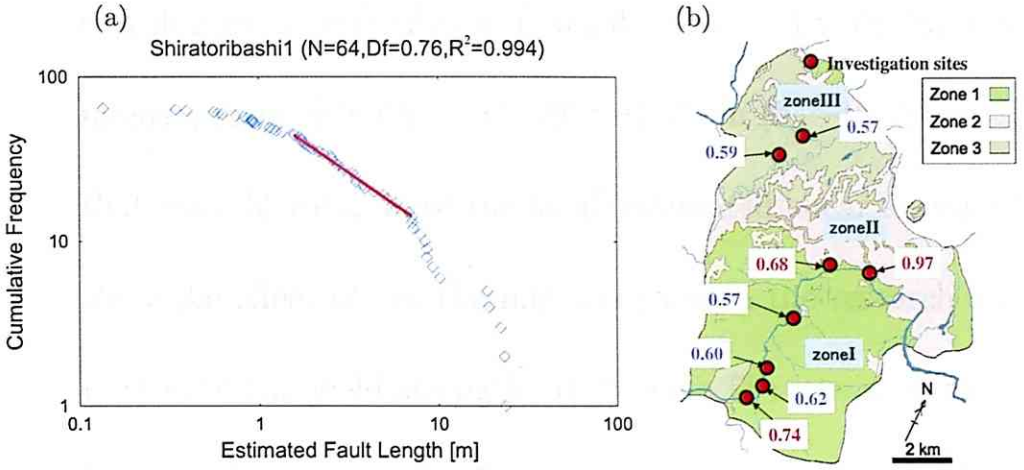

Fig.4-4 (a)Representative frequency distribution of the estimated fault length in Shiratori-bridge1. (b)Df-value of the estimated fault length in each investigation site. Df-value is proportional to the b-value of earthquake.

similar to D of thickness or length of the sealed crack. P,T and fluid condition of zone II metamorphic rock seems to have been suitable to create the fluid-filled cracks in the measured scale, supported that the number density of the sealed crack is largest in zone II (Table.3-1).

In a situation of Fig.4-3, a thickness W of the sealed crack is deemed a minimum value of the corresponding fault displacement D on a measured plane. Shear strain γ^*=D/L$_S$ is the commonly used parameter to characterize the shear motion in seismology and related to the inelastic yield strength of the material in the environment (Cowie and Sholz 1990). γ^* varies between 10^{-3}~10^{-1}, mostly in the range 5×10^{-3}~5×10^{-2} (Scholz and Cowie 1990). Estimated γ^* of the sealed crack ranges 10^{-7}~10^{-2} (Fig.4-5), where although the values are broadly more than 10^{-4} in meta-

morphic grade to (g)Yanase (zone II) consistent with that obtained in seismology, inconsistently small 10^{-6}〜10^{-5} in (h)〜(i) (zone III). The result that zone III rocks have the small estimated shear strain γ^* can directly show the effect of the thermal structure in the research area, since γ^* is related to the yield strength. If so, zone III rocks may have many micro-faults and micro-cracks followed by the sealing or healing. Not many micro sealed cracks are seen in thinsections of zone III rock with polarized microscope, suggesting that they might be smaller than μm scale or healing are main. Because small scale fractures in high temperature are considered to occur along grain boundaries not intruding grains, the scarless crack healing may be possible. As a result, the sealed crack number density in outcrops are smallest in zone III.

(i)Kamigenda

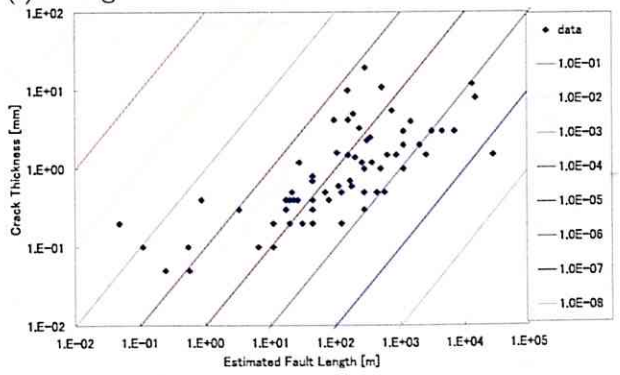

The rest of figure.4-5.
Estimated shear strain γ^* gets smaller value in Zone III region than in others.

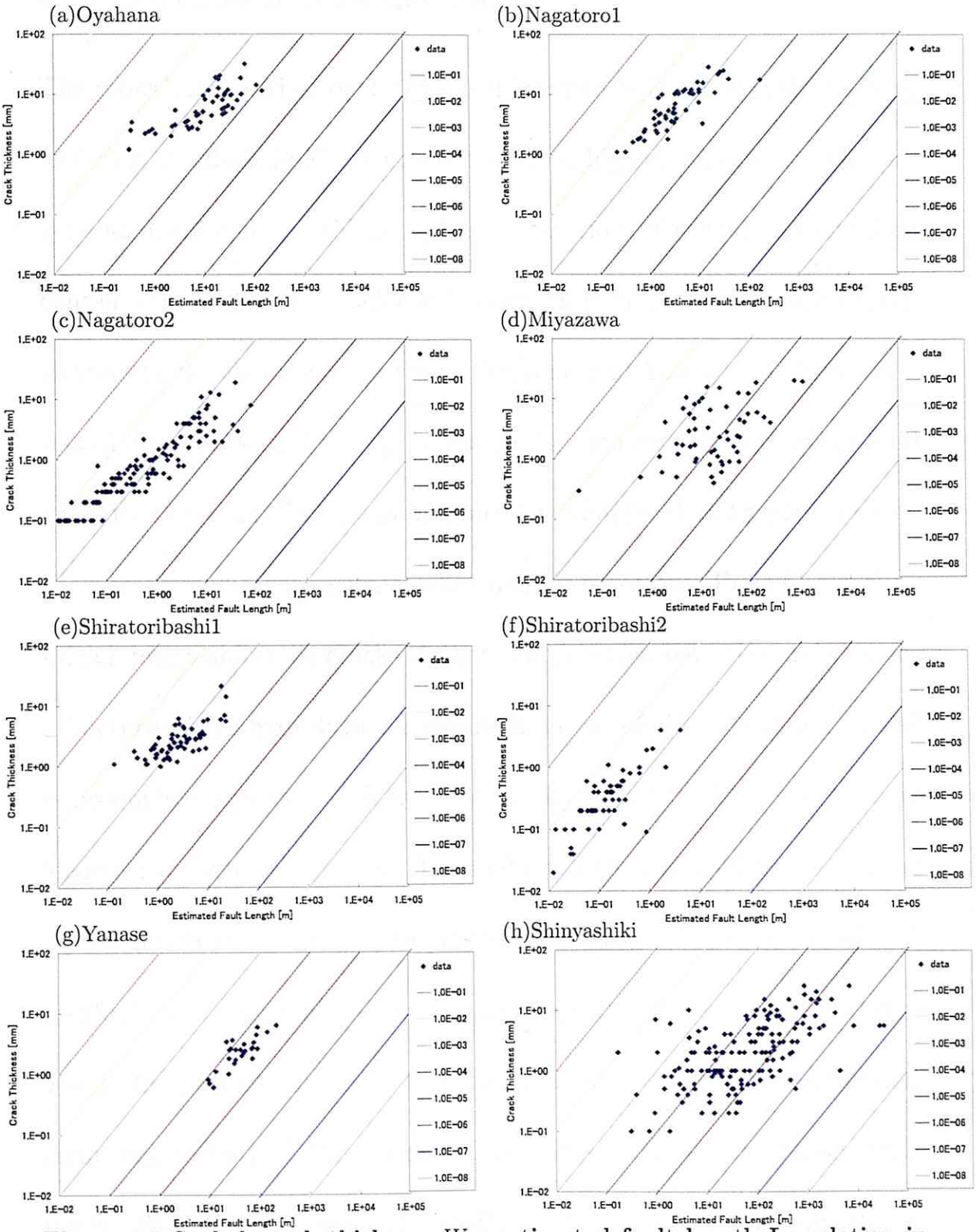

Figure.4-5 Sealed crack thickness W - estimated fault length L_S relation in each investigation site (a)~(i). Color lines correspond to the shear strain γ^* ($W = \gamma^* L_S$).

4.2 Fluid flow creating the crack

The growth mechanism of the cracks filled with fluid are thought positive feedback by which fluid are concentrated on high cracked regions by advection. Consequently the two phase separation with high and low fluid content region should be achieved, resulting in the observed sealed crack clusters in the metamorphic rocks. Toriumi and Yamaguchi (2000) presented an hydrological transport model for the crack cluster, where fluid are driven by the difference in pressure (Darcian flow) and passes through the porous media with permeability mainly by cracks (Fig.4-6). In their model, permeability by cracks is treated appropriately as the cubic law for a fracture with a hydrological aperture in viscous fluid approximation and is proportional to the crack number density which works as the positive feedback mechanism of fluid. They adupted the qualitative constitutive equation between reduced fluid pressure and the crack number density. It results in the temporal and spacial development of the crack systems in which the master equation of the crack number density have a non-linear term and scale- and time-invariant solutions of two-thirds power exponents. The clustering property predicted by the model is comparable to the result by Toriumi and Hara (1995), 0.7-0.9 fractal dimension in 1-D

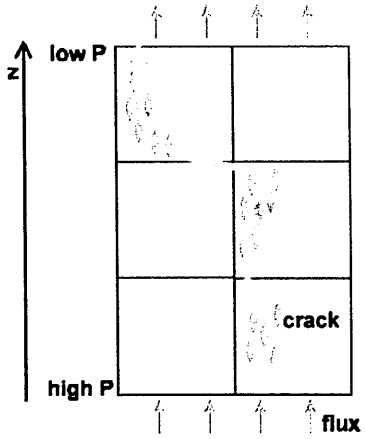

Fig.4-6 Hydrological transport model where fluid are driven by the difference in pressure and passes through the porous media with permeability mainly by cracks (Darcian flow). Fluid pressure P_f gets smaller in high water content region, which works as the positive feedback mechanism of fluid concentration.

for spacing.

The numerical calculations of the modified Toriumi and Yamaguchi (2000) model are computed here to investigate more details of the crack cluster formation, introducing more strong non-linear effect into the crack connection. Basic equations are law of conservation of mass

$$\frac{\partial}{\partial t}(\rho_{\mathrm{w}}\phi) = -\nabla \cdot (\rho_{\mathrm{w}}\phi\vec{v}\,) \tag{4.15}$$

and law of conservation of momentum (Darcy's law)

$$\overrightarrow{v} = -\frac{k}{\eta}\nabla P \tag{4.16}$$

where $\overrightarrow{v}$ is velocity of fluid, ρ_{w} is fluid (water) density, ϕ is porosity by

water-filled cracks, P is reduced fluid pressure, k is permeablity assumed here to be proportional to porosity ϕ ($k = m'\phi$), m' is a constant. Fundamental form of the coupling equation is nonlinear advection equation of fluid-filled crack density ϕ, where v and P are smaller in a region of larger ϕ. It seems to be essential for the positive feedback of fluid. Since unknown variables are ϕ, v and P, another constitutive equation between P and ϕ is required to solve them. Though it is derived originally from the external elastic framework of porous media, the simple internal qualitative relation in order to reproduce the positive feedback mechanism of fluid

$$\frac{\partial P}{\partial z} = -g\left[\frac{\rho_{\mathrm{r}} + \rho_{\mathrm{w}}}{2} - \frac{\rho_{\mathrm{r}} - \rho_{\mathrm{w}}}{2}\tanh(\frac{\phi - \phi_0}{2\varepsilon})\right] \tag{4.17}$$

is introduced here, where z is positive upward, ρ_{r} is density of intact rock, ϕ_0 is the criterion of porosity level for the mechanism, ε is the transition width of porosity level from low to high porosity region. It relies on the assumption that as ϕ gets larger beyound a threshold value, the cracks begin to connect mutually and fluid pressure gradient $\partial P/\partial z$ gets smaller drastically in the region (Fig.1-5). The functional form and coefficidents of (4.17) correspond to fluid pressure gradient $\partial P/\partial z = -\rho_{\mathrm{r}} g$ in $\phi \rightarrow 0$ and

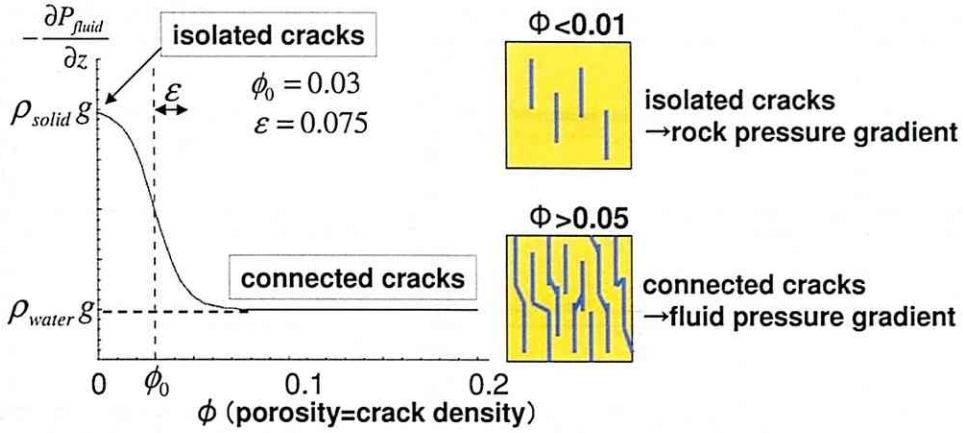

Fig.4-7 Illustration of a concept of eqs.(4.17). For low ϕ ($\phi \to 0$) cracks are isolated and crack fluid pressure are same as the surroundig rock. For high ϕ ($\phi > \phi_0$) cracks are connected and crack fluid pressure are same as water.

$-\rho_w g$ in $\phi \to 1$ (Fig.4-7).

Staggered cells are constructed for calculations, where ϕ and P are defined on the center of each cell and v on the boundary between two cells. Initial conditions are the perturbation of ϕ from the fixed value, low v value expected for Darcian flow, and P by (4.17). Boundary conditions at $z = 0$ are a little perturbated ϕ, v and P as same as the initial condition corresponding to a flux of fluid, and at the other boundary something additive need not be set up because a flux passes through simply. In addition to diffusion of momentum, an inevitable diffusion effect for computation are included. Space (z=0$\sim$1) are discretized into 1000 pieces and appropriate time step are choiced for 1-D calculations below.

The model cumputational results show the positive feed back of fluid

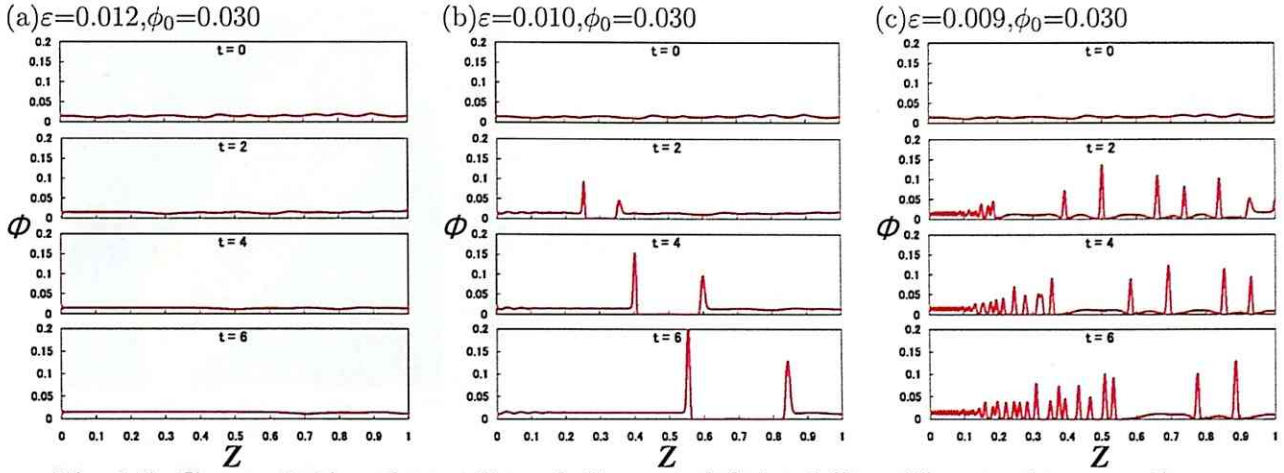

Fig.4-8 Computational results of the model in 1-D with varying on the parameters ε and ϕ_0. (a)ε=0.012, ϕ_0=0.030 (b)ε=0.010, ϕ_0=0.030 (c)ε=0.009, ϕ_0=0.030.

and the two phase separation structure which is caused even from nealy homogeneous initial condition, depending on the parameters ϕ, ε for non linear effect (Fig.4-8). There are some specific wave lengths of ϕ which can grow their amplitude, which are determined by the parameters non-linearly, too. Therefore the number of peaks of ϕ made from the initial perturbation are counted in the parameters range (Fig.4-9). The characteristic relation for the number of peaks of ϕ per unit distance between ϕ and ε are clearly seen, suggesting that ϕ and ε in natural system may be regulared by measuring the number density of the sealed cracks in natural rocks.

The characteristic relation between larger ϕ and smaller v, P in the connected fluid-filled crack cluster is essential for the autonomously formed

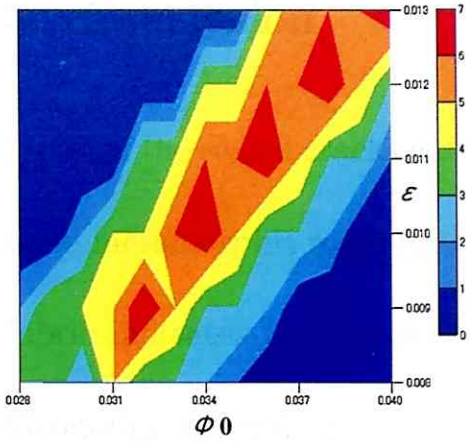

Fig.4-9 The number of peaks of ϕ made from the initial perturbation.

heterogeneous structure. Thus it is the confident reason fluid concentrates on the high fluid content region while fluid creates cracks, and can be indicative of the asperity stucture in the plate boundary.

5 Conclusion

Mode of the sealed cracks cutting schistosities in high angles in the Sanbagawa metamorphic rocks in the Kanto-Mountains are investigated. Microfabric indicates the repeated fractures and fluid transport of advection. Geometry depends mainly on metamorphic grade. Especially zone III rocks have the shear-faulting correlated sealed crack geometry inferred by the thermal structure. Size obeys the power-law in all investigation sites. The sealed cracks are clustering in 0.6-1.0 fractal dimension in 1-D scan line and correlate with the power-exponents of size. The characteristics of the sealed crack strongly shows the positive feedback mechanism of fluid which result in a cluster of the crack. Relatively high fluid-pressure perturbation caused by the connection of the cracks may make such a inhomogeneous structure realized by the model presented here. Asperity structures in the plate boundary can be understood by the difference in the pattern of the cracks filled with fluid. Fluid and deformation including earthquakes can be strongly coupled. Based on the mixed mode fracture model the corresponding fault length are estimated from thickness, length, and angle to the schistosity of the sealed crack. Estimated shear strain is comparable with earthquake except that in biotite zone.

b-value (shear crack statistics) estimated from the sealed crack statistics varies with a few kilometer scale. It is indicative of seismic b-value and asperity structure.

Acknowledgements

I gratefully acknowledge helpful discussions with Professor Toriumi in this paper. I would like to thank the member of Toriumi Laboratory for giving me useful suggestions and wide ranging passionate devotions.

References

[1] Lay T. and Kanamori H., 1980, Earthquake doublets in the solomon islands, Physics of the Earth and Planetary Interiors, 21, 283-304.

[2] Lay T. and Kanamori H., 1981, An asperity model of large earthquake sequences, in *Earthquake Prediction; An International Review*, edited by Simpson D.W. and Richards P.G., pp.579-592, AGU, Washington D.C.

[3] Aki K., 1984, Asperities, barriers, characteristic earthquakes and strong motion prediction, Journal of Geophysical Research, 89, 5867-5872.

[4] Cloos M., 1992, Thrust-type subduction zone earthquakes and seamount asperities; A physical model for seismic rupture, Geology, 20, 601-604.

[5] Sammis C.G., Nadeau R.M. and Johnson L.R., 1999, How strong is an asperity?, Journal of Geophysical Research, 104, 10609-10619.

[6] Johnson L.R. and Nadeau R.M., 2002, Asperity model of an earthquake: Static problem, Bulletin of the Seismological Society of America, 92, 672-686.

[7] Chen Y. and Sammis G., 2003, Asperity models for earthquakes, Bulletin of the Seismological Society of America, 93, 1792-1802.

[8] Yamanaka Y. and Kikuchi M., 2003, Source process of the recurrent Tokachi-oki earthquake on September 26, 2003, inferred from teleseismic body waves, Earth, Planets and Space, 55, e21-e24, 2003.

[9] Wells R.E., Blakely R.J., Sugiyama Y., Scholl D.W. and Dinterman P.A., 2003, Basin-centered asperities in great subduction zone earthquakes: A link between slip,

subsidence, and subduction erosion?, Journal of Geophysical Research, 108, 2507, doi:10.1029/2002JB002072.

[10] Seno T., 2003, Fractal asperities, invasion of barriers, and interplate earthquakes, Earth Planes Space, 55, 649-665.

[11] Okada T., Yaginuma T., Umino N., Kono T., Matsuzawa T., Kita S. and Hasegawa A., 2005, The 2005 M7.2 MIYAGI-OKI earthquake, NE Japan: Possible rerupturing of one of asperities that caused the previous M7.4 earthquake, Geophysical Research Letters, 32, L24302, doi:10.1029/2005GL024613.

[12] Sobiesiak M., Meyer U., Götze H.-J. and Krawczyk C.M., 2007, Asperity generating upper crustal sources revealed by b-value and isostatic residual anomaly grids in the area of Antofagasta, Chile, Journal of Geophysical Research, 112, B12308, doi:10.1029/2006JB004796.

[13] Brune J.N., 1968, Seismic moment, seismicity, and rate of slip along major fault zones, Journal of Geophysical Research, 73, 777-784.

[14] Bird P. and Kagan Y.Y., 2004, Plate-tectonic analysis of shallow seismicity: Apparent boundary width, beta, corner magnitude, coupled lithosphere thickness, and coupling in seven tectonic settings, Bulletin of the Seismological Society of America, 94, 2380-2399.

[15] Aki K., 1979, Characterization of barriers on an earthquake fault, Journal of Geophysical Research, 84, 6140-6148.

[16] Kawasaki I., 2004, Silent earthquakes occurring in a stable-unstable transition zone and implications for earthquake prediction, Earth Planets Space, 56, 813-821.

[17] Lei X.-L., Nishizawa O., Kusunose K., Cho A., Satoh T. and Nishizawa O., 2000, Compressive failure of mudstone samples containing quartz veins using rapid AE monitoring: the of asperities, Tectonophysics, 328, 329-340.

[18] Gutenberg R. and Richter C.F., 1944, Frequency of earthquakes in California, Bulletin of the Seismological Society of America, 34, 185-188.

[19] Ishimoto M. and Iida K., 1939, Observations of earthquakes registered with the microseismograph constructed recently, Bulletin of the Earthquake Research Institute University of Tokyo, 17, 531-544.

[20] Kanamori H. and Brodsky E., 2004, The physics of earthquakes, Reports on Progress in Physics, 67, 1429-1496.

[21] Abercrombie R.E., 1996, The magnitude-frequency distribution of earthquakes recorded with deep seismometers at Cajon Pass, Southern California, Tectonophysics, 261, 1-7.

[22] Abercrombie R.E., 1995, Earthquake source scaling relationships from 1- to 5 M_{L} using seismograms recorded at 2.5 km depth, Journal of Geophysical Research, 100, 24015-24036.

[23] Wiemer S. and Wyss M., 1997, Mapping the frequency-magnitude distribution in asperities; An improved technique to calculate recurrence times?, Journal of Geophysical Research, 102, 15115-15128.

[24] Hirose F., Nakamura A., and A. Hasegawa, 2002, b-value variation associated with the rupture of asperities - spatial and temporal distributions of b-value east off NE Japan, Zisin, 55, 249-260.

[25] Kawakatsu H. and Watada S., 2007, Seismic evidence for deep water transportation in the mantle, Science, 316, 1468-1471.

[26] Iwamori H., 2007, Transportation of H2O beneath the Japan and its implication for global water circulation, Chemical Geology, 239, 182-198.

[27] Hasegawa A., and Nakajima J., 2004, Geophysical constraints on slab subduction and arc magmatism, Geophysical Monograph, 150, 81-94.

[28] O'Connell R. and Budiansky B., 1974, Seismic velocities in dry and saturated cracked solids, Journal of Geophysical Research, 79, 5412-5426.

[29] Watanabe T., 1993, Effects of water and melt on seimic velocities and their application to characterization of seismic reflectors, Geophysical Research Letters, 20, 2933-2936.

[30] Takei Y., 2002, Effect of pore geometry on Vp/Vs; From equilibrium geometry to crack, Journal of Geophysical Research, 107, doi:10.1029/2001JB0000522.

[31] Husen S. and Kissling E., 2001, Postseimic fluid flow after the large subduction earthquake of Antofagasta, Chile, Geology, 29, 847-850.

[32] Shapiro S.A., Patzig R., Rothert E. and Rindschwentner J., 2003, Triggering of seismicity by pore pressure perturbations; Permeability-related signatures of the phenomenon, Pure and applied geophysics, 160, 1051.

[33] Hilgers C. and Urai J.L., 2005, On the arrangement of solid inclusions in fibrous veins and the role of the crack-seal mechanism, Journal of Structural Geology, 27, 481-494.

[34] Nollet S., Urai J.L., Bons P.D. and Hilgers C., Numerical simulations of polycrystal growth in veins, Journal of Structural Geology, 27, 217-230.

[35] Hilgers C., Dlig-Gruschinski K. and Urai J.L., 2003, Microstructures grown experimentally from advective supersaturated solution and their implication for natural vein systems, Journal of Geochemical Exploration, 78-79, 221-225.

[36] Nakashima Y., 1995, Transport model of buoyant metamorphic fluid by hydrofracturing in leaky rock, Journal of Metamorphic Geology, 13, 727-736.

[37] Okamoto A. and Toriumi M., 2005, Progress of actinolite-forming reactions in mafic schists during retrograde metamorphism; an example from the Sanbagawa metamorphic belt in central Shikoku, Japan, Journal of Metamorphic Geology, 23, 335-356.

[38] Toriumi M. and Inui M., 2001, Pressure-Temperature-Water production rate paths in the subduction metamorphism, Bulletin of the Earthquake Research Institute, University of Tokyo, 76, 367-376.

[39] Winstch R.P., Byrne T. and Toriumi M., 1999, Exhumation of the Sanbagawa blueschist belt, SW Japan, by lateral flow and extrusion; evidence from structural kinematics and retrograde P-T-t paths, Geological Society of London, Special Publication, 154, 129-155.

[40] Etheridge M.A., Wall V.J. and Cox S.F., 1984, High fluid pressures during regional metamorphism and deformation: implications for mass transport and deformation mechanism, Journal of Geophysical Research, 86, 4344-4358.

[41] M. Toriumi, and E. Hara, 1995, Crack geometries and deformation by the crack-seal mechanism in the Sambagawa metamorphic belt. Tectonophysics, 245, 249-261.

[42] M. Toriumi and H. Yamaguchi, 2000, Dehydration and the Mechanics of Metamorphic Belts, Journal of Geography, 109, 600-613.

[43] Guo Z. and Ogata Y., 1997, Statistical relations between the parameters of aftershocks in time, space, and magnitude, Journal of Geophysical Research, 102, 2857-2873.

[44] Vinciguerra S., 2002, Damage mechanics preceding the September-October 1989 flank eruption at Mount Etna volcano inferred by seismic scaling exponents, Journal of Volcanology and Geothermal Research, 113, 391-397.

[45] Higashino, T., 1975, Biotite zone of the Sanbagawa metamorphic terrain in the Shiragayama area, central Shikoku, Japan. Journal of the Geological Society of Japan, 81, 653-670.

[46] Higashino, T., 1990, The higher grade metamorphic zonation of the Sanbagawa metamorphic belt in central Shikoku, Japan, Journal of Metamorphic Geology, 8, 413-423.

[47] Enami, M., 1982, Oligoclase-biotite zone of Sambagawa belt in Bessi area, Central Shikoku, Japan, Journal of the Geological Society of Japan, 88, 887-900

[48] Takana K. and Fukuda M., 1974, Geologic structure and metamorphic zoning of the northern extremity of the Sanbagawa metamorphic terrain in the Kanto Mountains - with special reference to the occurrence of biotites -, Journal of Mineralogy, Petrology and Economic Geology, 69, 313-323

[49] Sakai, C., 1980, Biotite zone in the Sanbagawa metamorphic terrain east of Onishimachi, Kanto Mountains, Journal of the Geological Society of Japan, 86, 517-524

[50] Tokuda, M., 1986, The research of geological structure in the Kanto Mountains of Sambagawa metamorphic belt and Chichibu belt, Geological report of the Hiroshima University, 26, 195-260

[51] Hashimoto, M. and Funakoshi, R., 1991, Amphiboles of basic schists in the Sambagawa metamorphic terrain of the Kodama-Nagatoro area, Kanto Mountains, Journal of Mineralogy, Petrology and Economic Geology, 86, 497-506

[52] Hashimoto M., Tagiri, M., Kusakabe K., Masuda K., and Yano, T., 1992, Geologic structure formed by tectonic stacking of sliced layers in the Sanbagawa metamorphic terrain, Kodama-Nagatoro area, Kanto Mounttains, Journal of the Geological Society of Japan, 98, 953-965

[53] Yano, T., and Tagiri, M., 1998, Geological and thermal structure of Sanbagawa metamorphic belt in the Sanbagawa river and Ayukawa river area, Kanto Mountains, Journal of the Geological Society of Japan, 104, 452-453

[54] Miyashita, A., Re-examination of "Geologic structure formed by tectonic stacking of sliced layer" in the Sanbagawa metamorphic rocks, Kanto Mountains, Journal of the Gelogical Society of Japan, 104, 731-746

[55] Abe, T., Takagi, H., Shimada, K., Kimura, S., Ikeyama, K., Miyashita, A., Ductile shear deformation of the Sambagawa metamorphic rocks in the Kanto Mountains, Journal of Geological Society of Japan, 107, 337-353

[56] Tagiri, T., Matsumoto, T., and Tanimoto, K., 2003, Reevaluation of the precision of the degree of graphitization, and the boundaries between shuffled-cards in the Sanbagawa metamorphic belt, Kanto Mountains, Japan, Journal of Mineralogical and Petrological sciences, 32, 175-184

[57] Toriumi, M., 1975, Petrological study of the Sambagawa metamorphic rocks, Kanto Mountains, central Japan, The University Museum, the University of Tokyo, Bulletin, no.9

[58] Hirajima, T., Isono, T., and Itaya, T., 1992, K-Ar age and chemistry of white mica in the Sanbagawa metamorphic rocks in the Kanto Mountains, central Japan, Journal of the Geological Society of Japan, 98, 445-455

[59] Miyashiro, A., 1994, Metamorphic petrology, UCL Press, London, 404p

[60] Banno, S., Sakai, C., and Higashino, T., 1986, Pressure-temperature trajectory of the Sanbagawa metamorphism deduced from garnet zoning. Lithos, 19, 51-63.

[61] Otsuki, M., and Banno S., 1990, Prograde and retrograde metamorphism of hematite-bearing basic schists in the Sambagawa Belt in central Shikoku, Journal of Metamorphic Geology, 8, 425-439.

[62] Nakamura, C., and Enami, M., 1994, Prograde amphiboles in hematite-bearing basic and quartz schists in the Sambagawa belt, central Shikoku - relationship between metamorphic field gradient and P-T paths of individual rocks, Journal of Metamorphic Geology, 12, 841-852.

[63] Enami, M., 1998, Pressure-Temperature path of Sanbagawa prograde metamorphism deduced from grossular zoning of garnet, Journal of Metamorphic Geology, 16, 97-106.

[64] Banno, Y., 2000, Intermediate high-pressure exhumation of the northern segment of the Sanbagawa belt, Saruta-gawa area, central Shikoku, Japan, Lithos, 50, 289-303.

[65] Tagiri, M., Yago, Y., and Tanaka, A., 2000, Shuffled-cards structures and different P/T conditions in the Sanbagawa metamorphic belt, Sakuma-Tenryu area, central Japan, The Island Arc, 9, 188-203.

[66] Okamoto, A., and Toriumi, M., 2001, Application of differential thermodynamics (Gibbs' method) to amphibole zonings in the metabasic system, Contributions to Mineralogy and Petrology, 141, 268-286

[67] Okamoto, A., and Toriumi, M., 2004, Optimal mixing properties of calcic and subcalcic amphiboles: application of Gibbs' method to the Sanbagawa schists, SW Japan, Contributions to Mineralogy and Petrology, 146, 529-545

[68] Inui, M., and Toriumi, M., 2002, Prograde pressure-temperature paths in the pelitic schists of the Sambagawa metamorphic belt, SW Japan, Journal of Metamorphic Geology, 20, 563-580

[69] Enami, M., 1983, Petrology of pelitic schists in the oligoclase-biotite zone of the Sanbagawa metamorphic terrain, Japan: phase equilibria in the highest grade zone of a high-pressure intermediate type of metamorphic belt, Journal of Metamorphic Geology, 1, 141-161

[70] Enami, M., and Wallis, R.S., and Banno, Y., 1994, Paragenesis of sodic pyroxene-bearing quarts schists: implications for the P-T history of the Sanbagawa belt, Contributions to Mineralogy and Prtrology ,116 ,182-198

[71] Aoya, M., Uehara, S., Matsumoto, M., Wallis, S.R., and Enami, M., 2003, Subduction-stage pressure-temperature path of eclogite from the Sambagawa belt: Prophetic record for oceanic-ridge subduction, Geology, 31, 1045-1048

[72] Peacock, S.M., and Wang, K., Seismic consequences of warm versus cool subduction metamorphism: Examples from southwest and northeast Japan, Science, 286, 937-939

[73] Iwamori, H., 2000, Thermal effects of ridge subduction and its implications for the origin of granitic batholith and paired metamorphic belts, Earth and Planetary Science Letters, 181, 131-144

[74] Suyari, K., Kuwano, Y., and Ishida, K., 1980a, Stratigraphy and geological structure of the Mikabu Green-rock terrain and its environs, Jour. Sci. Tokushima Univ., 13, 63-82

[75] Suyari, K., Kuwano, Y., and Ishida, K., 1980b, Discovery of the late triassic conodonts from the Sanbawaga metamorphic belt proper in western Shikoku, Jour. Geol. Soc. Japan, 86, 827-828

[76] Iwasaki, M., Ichikawa, K., Yao, S., and Faure, M., 1984, Fossil ages of green rock conglomerates from Mikabu green schists in eastern Shikoku, Japan, Report of Kansai Group, Geological society of Japan, 97, 21-21

[77] Fujimoto, H., 1939, Radiolarian remains discovered in a crystalline schist of the Sambagawa System, Proceedings of the Imperial Academy, 14, 252-254

[78] Fujimoto, H., and Yamada, J., 1949, Discovery of a Crinoid-limestone in a crystalline schist of the Nagatoro system of the Kwanto Mountainland, Proceedings of the Japan Academy, 25, 175-178

[79] Guidi, A., Charvet, J. and Sato, T., 1984, Finding of granitic olistoliths and pre-Cretaceous radiolarians in the northwestern Kanto Mountains, Cunma Prefecture, central Japan, Jour. Geol. Soc. Japan, 90, 853-856

[80] Itaya, T., and Takasugi, H., 1988, Muscovite K-Ar ages of the Sambagawa schists, Japan and argon depletion during cooling and deformation, Contrib. Mineral. Petrol. 100, 281-290

[81] Takasu, A., and Dallemeyer, R.D., 1990, 40Ar/39Ar mineral age constraints for the tectonothermal evolution of the Sambagawa metamorphic belt, central Shikoku, Japan, a Cretaceous accretionary prism, Tectonophysics, 185, 111-139

[82] Isozaki, Y., and Itaya, T., 1990, Chronology of Sambagawa metamorphism, Journal of Metamorphic Geology,8, 401-411

[83] Toriumi, M., 1982, Strain stress and uplift, Tectonics, 1, 57-76

[84] Faure, M., 1983, Eastward ductile shear during the early tectonic phase in the Sanbagawa belt, Journal of the Geological Society of Japan, 89, 319-329

[85] Faure, M. 1985, Microtectonic evidence for eastward ductile shear in the Jurassic orogen of SW Japan, Journal of Structural Geology, 7, 175-186

[86] Shimizu, I., and Yoshida, S., 2004, Strain geometries in the Sanbagawa metamorphic belt inferred from deformation structures in metabasite, Island Arc, 13, 95-109

[87] Hara, I., Hide, K., Takeda, K., Tsukuda, E., Tokuda, M., and Shiota, T., 1977, Tectonic movement in the Sambagawa Belt, The Sambagawa belt (ed. Hide, K.), Hiroshima University Press, 307-390

[88] Toriumi, M., and Noda, H., 1986, The origin of strain patterns resulting from contemporaneous deformation and metamorphism in the Sambagawa metamorphic belt, Journal of Metamorphic Geology, 4, 409-420

[89] Shimizu, I., 1988, Ductile deformation in the low-grade part of the Sambagawa metamorphic belts in the northern Kanto Mountains, Central Japan, Journal of Geological Society of Japan, 94, 609-628

[90] Hara, I., Shiota, T., Hide, K., Okamoto, K., Takeda, K., Hayasaka, Y. and Sakurai, Y., 1990, Nappe structure of the Sambagawa belt, Journal of Metamorphic Geology, 8, 441-456

[91] Hara, I., Shiota, T., Hide, K., Kanai, K., Goto, M., Seki, S., Kaikiri, K., Takeda, K., Hayasaka, Y., Miyamoto, T., Sakurai, Y., and Ohtomo, Y., 1992, Tectonic evolution of the Sambagawa schists and its implications in convergent margin processes, Journal of science of the Hiroshima University Series C, Geology and mineralogy, 9, 495-595

[92] Wallis, S., Banno, S., and Radvanec, M., 1992, Kinematics, structure and relationship to metamorphism of the east-west flow in the Sanbagawa Belt, South-west Japan, The Island Arc, 1, 176-185

[93] Toriumi, M., 1985, Two types of ductile deformation / regional metamorphic belt, Tectonophysics, 113, 307-326

[94] Banno, S., Higashino, T., Otsuki, M., Itaya, T., and Nakajima, T., 1978, Thermal structure of the Sanbagawa metamorphic belt in central Shikoku, Journal of Physics of the Earth, 26, 335-345

[95] Banno, S., and Sakai, C., 1989, Geology and metamorphic evolution of the Sambagawa metamorphic belt, Japan, Evolution of Metamorphic Belts, Geological Society Special Publication, 43, 519-532

[96] Wallis, S.R., 1990, The timing of folding and stretching in the Sambagawa Belt, the Asemigawa region, Central Shikoku, Journal of the Geological Society of Japan, 96, 345-352

[97] Takasu, A., Wallis, S.R., Banno, S., and Dallmeyer, R.D., 1994, Evolution of the Sambagawa metamorphic belt, Japan, Lithos, 33, 119-133.

[98] Oliver N.H.S. and Bons P.D., 2001, Mechanisms of fluid flow and fluid-rock interaction in fossil metamorphic hydrothermal systems inferred from vein-wallrock patterns, geometry and microstructure, Geofluids, 137-162.

[99] Durney D.W., 1976, Pressure-solution and crystallization deformation, Philosophical Transactions of the Royal Society, A., 283, 229-240.

[100] Raj R., 1982, Creep in polycrystalline aggregates by matter transport through a liquid phase, Journal of Geophysical Reseach, 87, 4731-4739.

[101] Rutter E.H., 1983, Pressure solution in nature, theory and experiment, Journal of Geological Soceity of London, 140, 725-740.

[102] Drury M.R. and Urai J.L., 1990, Deformation-related recrystallization processes, Tectonophysics, 172, 235-253.

[103] Rye D.M. and Bradbury H.J., 1988, Fluid flow in the crust; an example from a Pyrenean thrust ramp, American Journal of Science, 288, 197-235.

[104] Weertman J., 1971, Theory of water-filled crevaces in glaciers applied to vertical magma transport beneath ocean ridges, Journal of Geophysical Reseach, 85, 9543-9559.

[105] Secor D.T. and Pollard D.D., 1975, On the stability of open hydraulic fractures in the Earth's crust, Geophysical Research Letters, 2, 510-513.

[106] Pollard D.D., 1977, Derivation and evaluation of a mechanical model for sheet intrusions, Tectonophysics, 19, 233-269.

[107] Takada A., 1990, Experimental study on propagation of liquid filled crack in gelatin; shape and velocity in hydrostatic stress condition, Journal of Geophysical Research, 95, 8471-8481.

[108] Davies J.H., 1999, The role of hydraulic fractures and intermediate-depth earthquakes in generating subduction-zone magmatism, Nature, 398, 142-145.

[109] Bons P.D., 2001, The formation of large quartz veins by rapid ascent of fluids in mobile hydrofractures, Tectonophysics, 336, 1-17.

[110] Fournier R.O. and Potter R.W., 1982, An equation correlating the solubility of quartz in water from 25° to 900°C at pressures up to 10000bars, *Geochimica et cosmochimica Acta*, 46, 1969-1973.

[111] Bowers, T.S., 1995, Pressure-volume-Temperature Properties of H2O-CO2 Fluids. *In: Bhrens, T.J. (ed.), Rock Physics and Phase Relations, A Handbook of Physical Constants, AGU Reference Shelf 3, AGU, Washington*, 47-72.

[112] Connolly J.A.D., 1997, Mid-crustal focussed fluid movement thermal consequences and silica transport, *In: Jamtveit B. and Yardley B.W.D. (eds.), Fluid flow and transport in rocks, Chapman and Hall, London*, 235-250.

[113] Atkinson B.K. and Meredith P.G., 1987, Experimental fracture mechanics data. In; Atkinson B.K. (Ed.), Fracture mechanics of rock. Academic press limited, pp. 477-525.

[114] Nara Y. and Kaneko K., 2006, Sub-critical crack growth in anisotropic rock, International Journal of Rock Mechanics and Mining Sciences, 43, 437-453.

[115] McCaffrey K., Johnston J.D. and Feely M., 1993, Use of fractal statistics in the analysis of Mo-Cu mineralization at Mace Head, Country Galway, Irish Journal of Earth Sciences, 12, 139-148.

[116] Johnston J.D., 1993, Three-dimensional geometries of veins and their relationship to fold: Examples from the Carboniferous of eastern Ireland, Irish Journal of Earth Sciences, 12, 47-63.

[117] Fisher D.M., Brantley S.L., Everett M. and Dzvonik J., 1995, Cyclic fluid flow through a regionally extensive fracture network within the Kodiak accretionary prism, Journal of Geophysical Research, 100, 12881-12894.

[118] Clark M.B., Brantley S.L., and Fisher D.M., 1995, Power-law vein thickness distributions and positive feedback in vein growth. Geology, 23, 975-978.

[119] Simpson G.D.H., 2000, Synmetamorphic vein spacing distributions: Characterisation and origin of a distribution of veins from NW Sardinia, Italy, Journal of Structural Geology, 22, 335-348.

[120] Ortega O. and Marrett R., 2000, Prediction of macrofracture properties using microfracture information, Mesaverde Group sandstones, San Juan basin, New Mexico, Journal of Structural Geology, 22, 571-588.

[121] Foxford K.A., Nicholson R., Polya D.A. and Hebblethwaite R.P.B, 2000, Extensional failure and hydraulic valving at Minas da Panasqueira, Portugal: Evidence from vein spatial distributions, displacements and geometries, Journal of Structural Geology, 22, 1065-1086.

[122] Laubach S.E. and Meghan E.W., 2006, Diagenesis in porosity evolution of opening-mode fractures, Middle Triassic to Lower Jurassic La Boca Formation, NE Mexico, Tectonophysics, 419, 75-97.

[123] Ijiri Y. and Simon H.A., 1977, Skew distributions and the sizes of business firms, Amsterdam, North-Holland Publishing Company, 231p.

[124] Mandelbrot B.B., 1983, The fractal geometry of Nature; San Francisco, W.H. Freeman, 468p.

[125] Scholz C.H. and Cowie P.A., 1990, Determination of total strain from faulting using slip measurements, Nature, 346, 837-839.

[126] Bons P.D., 2000, The formation of veins and their microstructures, *In: Stress, Strain and Structure, A volume in honour of W.D. Means, Eds: M.W.Jessell and J.L.Urai*, Journal of the Virtual Explorer, 2.

[127] Cox S.F. and Etheridge M.A., 1983, Crack-seal fibre growth mechanisms and thier relationship to displacement paths, Journal of Structural Geology, 9, 779-788.

[128] A. Okamoto, T. Kikuchi, and N. Tsuchiya, 2008, Mineral distribution within polymineralic veins in the Sanbagawa belt, Japan: implications for mass transfer during vein formation. Contribution to Mineralogy and Petrology, 156, 323-336.

[129] Ramsay, J.G., 1980, The crack-seal mechanism of rock deformation. Nature, 284, 135-139.

[130] Vermilye J.M. and Scholz C.H., 1995, Relations between vein length and aperture, Journal of Structural Geology, 238, 423-434.

[131] Olson J.E., 2003, Sublinear scaling of fracure aperture versus length: an exception or thr rule?, Journal of Geophysical Reseach, 108, 2413, doi:10.1029/2001JB000419.

[132] Erdogan F. and Sih G.C., 1963, Transactions of the ASME; series D; Journal of Basic Engineering, 85, 519-

[133] Nüchter J.A and Stöckhert B., 2007, Vein quartz microfabrics indicating progressive evolution of fractures into cavities during postseismic creep in the middle crust, Journal of Structural Geology, 29, 1445-1462.

[134] Pollard D.D. and Segall P., 1987, Theoretical displacements and stresses near fractures in rock; with applications to faults, joints, veins, dikes, and solution surfaces; In Atkinson B.K. (Ed.), Fracture Mechanics of Rock, Academic Press, London, pp.277-350.

[135] Delaney P.T. and Pollard D.D., 1981, Deformation of host rocks and flow of magma during growth of Minette dikes and breccia-bearing intrusions near Ship Rock, New Mexico, U.S. Geological Survey Professional Papers, 1202, 1-61.